Photolysis frequency of O_3 to $O(^1D)$: Measurements and modeling during the International Photolysis Frequency Measurement and Modeling Intercomparison (IPMMI)

A. Hofzumahaus,[1] B. L. Lefer,[2] P. S. Monks,[3] S. R. Hall,[2] A. Kylling,[4] B. Mayer,[2,5] R. E. Shetter,[2] W. Junkermann,[6] A. Bais,[7] J. G. Calvert,[2] C. A. Cantrell,[2] S. Madronich,[2] G. D. Edwards,[3,8] A. Kraus,[1,9] M. Müller,[1,10] B. Bohn,[1] R. Schmitt,[11] P. Johnston,[12] R. McKenzie,[12] G. J. Frost,[13] E. Griffioen,[14] M. Krol,[15] T. Martin,[6,16] G. Pfister,[16,8] E. P. Röth,[17,18] A. Ruggaber,[19] W. H. Swartz,[20] S. A. Lloyd,[20] and M. Van Weele[21]

Received 6 November 2003; revised 13 February 2004; accepted 23 February 2004; published 24 April 2004.

[1] The International Photolysis Frequency Measurement and Modeling Intercomparison (IPMMI) took place at Boulder, Colorado, from 15 to 19 June 1998 and offered the opportunity to test how well experimental techniques and theoretical models can determine the photolysis frequency of $O_3 \rightarrow O(^1D)$ in the troposphere. Different techniques measured the downwelling 2π sr component of $j(O^1D)$ at the ground and were blindly compared to each other. Moreover, theoretical $j(O^1D)$ model results were blindly compared to data measured under clear sky at relatively low aerosol optical density. Six experimental groups operated one chemical actinometer (CA), six spectroradiometers (SR), and four filter radiometers (FR). General good agreement with deviations less than 10% among the radiometers (SR and FR) was found for solar zenith angles (SZA) less than 60°, provided that the instruments used similar absorption cross sections, quantum yields, and temperatures for deriving $j(O^1D)$. The deviations were generally larger at high solar zenith angles and reached a factor of 2 in some cases. Two spectroradiometers and one filter radiometer showed excellent agreement with each other and with the chemical actinometer at all solar zenith angles up to at least 80° within typically 5%. These radiometers used recently published $O(^1D)$ quantum yield data and explicitly considered the temperature dependence of $j(O^1D)$. This good agreement shows that each of the different categories of instruments (CA, SR, and FR) is in principle capable of accurate determinations of $j(O^1D)$. A large sensitivity was found to the choice of data for the $O(^1D)$ quantum yield. The best agreement between spectroradiometry and chemical actinometry was obtained when recently published quantum yield data were used. The IPMMI study thus supports the quantum yield recommendation by National Aeronautics and Space Administration-Jet Propulsion Laboratory [*Sander et al.*, 2003] and International Union of Pure and Applied Chemistry (IUPAC) (http://www.iupac-kinetic.ch.cam.ac.uk; data sheet POx2 from 2001). Fifteen models that were operated by 12 model groups participated in the comparison of modeled $j(O^1D)$ with measured data. Most models agreed within 15%

[1]Institut für Chemie und Dynamik der Geosphäre, Institut II: Troposphäre, Forschungszentrum Jülich, Jülich, Germany.
[2]Atmospheric Chemistry Division, National Center for Atmospheric Research, Boulder, Colorado, USA.
[3]Department of Chemistry, University of Leicester, Leicester, UK.
[4]Norwegian Institute for Air Research, Kjeller, Norway.
[5]Now at Deutsches Zentrum für Luft- und Raumfahrt, Oberpfaffenhofen, Germany.
[6]Institut für Meteorologie und Klimaforschung, Forschungszentrum Karlsruhe, Garmisch-Partenkirchen, Germany.
[7]Laboratory of Atmospheric Physics, Aristotle University of Thessaloniki, Thessaloniki, Greece.
[8]Now at Atmospheric Chemistry Division, National Center for Atmospheric Research, Boulder, Colorado, USA.
[9]Now at Grünenthal GmbH, Aachen, Germany.
[10]Now at Dresdner Bank, Frankfurt, Germany.
[11]Meteorologie Consult GmbH, Glashütten, Germany.
[12]National Institute of Water and Atmospheric Research, Lauder, New Zealand.
[13]Cooperative Institute for Research in Environmental Sciences, University of Colorado, Boulder, USA.
[14]Meteorological Service of Canada, Toronto, Canada.
[15]Institute for Marine and Atmospheric Research, Utrecht, Netherlands.
[16]Karl-Franzens Universität, Graz, Austria.
[17]Institut für Chemie und Dynamik der Geosphäre, Institut I: Stratosphäre, Forschungszentrum Jülich, Jülich, Germany.
[18]Institut für Physikalische Chemie, Universität Gesamthochschule Essen, Essen, Germany.
[19]Meteorologisches Institut, Universität München, Munich, Germany.
[20]Johns Hopkins University, Applied Physics Laboratory, Laurel, Maryland, USA.
[21]Royal Netherlands Meteorological Institute, DeBilt, Netherlands.

0148-0227/04/2003JD004333

with the spectroradiometer-derived $j(O^1D)$ values under clear sky at SZA < 75°, provided that they used similar absorption cross sections, quantum yields, and temperatures. While most models simulated the measured actinic flux quite well, significant deviations in $j(O^1D)$ were observed in cases when outdated $O(^1D)$ quantum yield data or inappropriate temperature data were used. *INDEX TERMS:* 0360 Atmospheric Composition and Structure: Transmission and scattering of radiation; 0365 Atmospheric Composition and Structure: Troposphere—composition and chemistry; 0394 Atmospheric Composition and Structure: Instruments and techniques; *KEYWORDS:* photolysis frequency, ozone, $O(^1D)$, measurement, radiative transfer modeling, intercomparison

Citation: Hofzumahaus, A., et al. (2004), Photolysis frequency of O_3 to $O(^1D)$: Measurements and modeling during the International Photolysis Frequency Measurement and Modeling Intercomparison (IPMMI), *J. Geophys. Res.*, *109*, D08S90, doi:10.1029/2003JD004333.

1. Introduction

[2] Photodissociation of atmospheric molecules by solar radiation plays a fundamental role in atmospheric chemistry. The photodissociation of trace species such as ozone and formaldehyde contributes to their removal from the atmosphere, but probably the most important role played by these photoprocesses is the generation of highly reactive atoms and radicals. Photodissociation of trace species and the subsequent reaction of the photoproducts with other molecules is the prime initiator and driver for the bulk of tropospheric chemistry. Of the range of photodissociation processes of importance in atmospheric chemistry, one of the most fundamental is the photolysis of ozone (O_3) yielding electronically excited $O(^1D)$ atoms [*Levy*, 1972]. Photolysis of ozone by ultraviolet light in the presence of water vapor is the main source of hydroxyl radicals in the troposphere, the primary tropospheric oxidant [*Ehhalt et al.*, 1991; *Levy*, 1974]:

$$\text{(R1)} \qquad O_3 + h\nu \longrightarrow O(^1D) + O_2\left(^1\Delta_g, {}^3\Sigma_g^-\right),$$

$$\text{(R2)} \qquad O(^1D) + H_2O \longrightarrow OH + OH.$$

The fate of the bulk of the $O(^1D)$ atoms produced via reaction (R1) is collisional quenching back to ground state oxygen atoms viz

$$\text{(R3)} \qquad O(^1D) + N_2 \longrightarrow O(^3P) + N_2,$$

$$\text{(R4)} \qquad O(^1D) + O_2 \longrightarrow O(^3P) + O_2.$$

The fraction of $O(^1D)$ atoms that form OH is dependent on the concentrations of H_2O, for example in the marine boundary layer about 10% of $O(^1D)$ formed go onto generate OH. The rate at which process (1) occurs is often expressed by analogy with a first-order rate coefficient, i.e.,

$$j(O^1D) = \frac{1}{[O_3]} \frac{d[O(^1D)]}{dt}, \qquad (1)$$

where $j(O^1D)$ is the photolysis frequency (s^{-1}), also referred to as j value. In order to calculate a photolysis frequency, the following equation can be evaluated for a molecule

$$j = \int \sigma(\lambda, T)\phi(\lambda, T)F(\lambda)d\lambda, \qquad (2)$$

where σ is the absorption cross section of the molecule and ϕ is the quantum yield for the photoprocess. It is important to note that both σ and ϕ are temperature (T) dependent in case of reaction (R1). The final term in equation (2) is $F(\lambda)$, the so-called spectral actinic flux, which quantifies the in situ radiation available to a molecule from all directions for the initiation of a photodissociation process [e.g., see *Madronich*, 1987]. Typical spectral photolysis frequencies ($\sigma\phi F$) calculated using equation (2) for $j(O^1D)$ are shown in Figure 1 (bottom) at two different solar zenith angles (SZA) representing high- (SZA = 16°) and low-Sun (SZA = 75°) conditions. The spectral distributions of $j(O^1D)$ are limited at short wavelengths by the available ultraviolet radiation and at long wavelengths by the decreases of σ and ϕ. It is evident that at low Sun the spectral photolysis frequency is smaller in magnitude and its distribution is shifted toward longer wavelengths. The attenuation and shift are mainly consequences of the UV-absorption by the overhead atmospheric ozone, which has a stronger effect at high SZA when the path of the photons is longer through the atmosphere.

[3] There are two main groups of experimental methods used for the determination of $j(O^1D)$. The first is chemical actinometry (CA), a method of detecting actinic flux using the chemical species of interest. Chemical actinometry is a direct measure of a photolysis frequency [e.g., *Shetter et al.* 1996], as the molecule of interest is exposed to the incident solar radiation and the build-up rate of the photodissociation product (or some proxy) is measured by a suitable detection method. An advantage of actinometry is that it does not depend on the knowledge of σ and ϕ, but it does depend on a chemical calibration for the concentration of a reactant and a photoproduct (or proxy). Experimentally, chemical actinometers involve measuring the photolysis frequency in a flowing or static system. There is a requirement for properly characterized fields of view for these techniques in order to acquire incident actinic flux exposures.

[4] The second group of techniques used to measure $j(O^1D)$ are radiometers. In this case the photolysis frequency is derived from the intensity of the incident

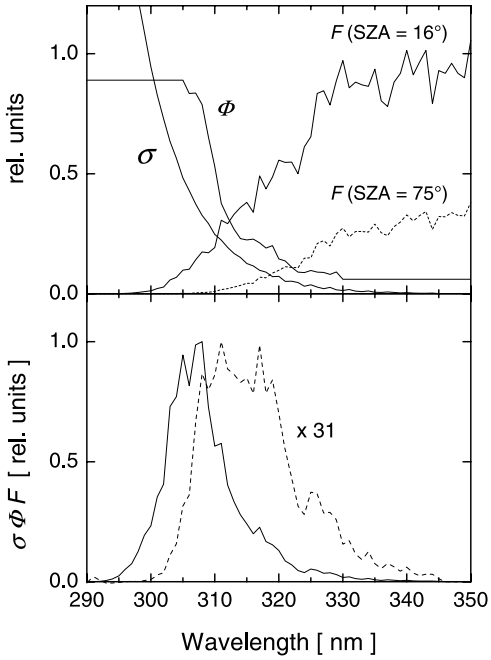

Figure 1. (top) Wavelength dependencies of the absorption cross section of O_3 (σ) and $O(^1D)$ quantum yield from the photolysis of O_3 (ϕ) at 298 K, and the actinic flux $F(\lambda)$ at two different solar zenith angles (SZA). The σ (in units of 4.2×10^{-19} cm^2) is from *Malicet et al.* [1995], ϕ is from *Talukdar et al.* [1998], and $F(\lambda)$ (in units of 1.67×10^{14} cm^{-2} s^{-1} nm^{-1}) was measured by Forschungszentrum Jülich during IPMMI on 19 June. (bottom) Spectral distribution of $j(O^1D)$ at SZA = 16° (solid line; median at 307 nm) and SZ*A* = 75° (dashed line; median at 315 nm). The $\sigma\phi F$ is given in units of 3×10^{-6} s^{-1} nm^{-1}.

radiation detected by a photoelectric device. The methods of optical collection vary from flat plate devices having a cosine-dependent angular response to hemispherical input optics with an isotropic angular response. Flat plate devices are sensitive to irradiance and require a number of complex corrections in order to determine actinic flux [e.g., *McKenzie et al.*, 2002], whereas the isotropic hemispherical optics monitor 2π sr actinic flux directly [e.g., *Junkermann et al.*, 1989]. The two main subsets of radiometry instrumentation are spectroradiometry (SR) and so called fixed-bandwidth or filter radiometry (FR). Spectroradiometry measures the relevant spectrally resolved absolute intensity of the actinic flux and uses equation (2) to determine the photolysis frequency [e.g., *Hofzumahaus et al.*, 1999]. This method requires an absolute calibration of the intensity of the radiation and knowledge of the relevant molecular parameters σ and ϕ. In filter radiometry, an appropriate optical wavelength selection is chosen to mimic the spectral function ($\sigma\phi$) of the relevant photolysis frequency by means of an optical filter and a photodetector [e.g., *Junkermann et al.*, 1989]. Ideally, the signal of a filter radiometer would be directly proportional to the photolysis frequency. However, in all practical cases the spectral response of the radiometer does not match exactly the shape of $\sigma(\lambda)\phi(\lambda)$. As a result the relationship between $j(O^1D)$ and the radiometer signal exhibits nonlinearities as the spectral distribution of the ultraviolet flux changes with overhead ozone column and solar zenith angle [e.g., *Bohn et al.*, 2004]. The use of fixed-bandwidth methods further complicates the determination of $j(O^1D)$ owing to the temperature dependence of σ and ϕ, which is not accounted for by the filter radiometer. The filter radiometric method requires an absolute calibration versus another absolute measurement technique (e.g., chemical actinometer) or of the intensity of the radiation. Moreover, it is important to measure the spectral response of a $j(O^1D)$ filter radiometer and to know the relevant molecular parameters (compare equation (2)).

[5] In the troposphere, $j(O^1D)$ is highly variable in space and time owing to the influences of many varying atmospheric parameters. So far, in situ measurement methods (Table 1) have yielded data only in a few places and times. For this reason, atmospheric chemistry models usually rely on photolysis frequency coefficients that are derived from modeled radiation fields. These are determined by means of radiative transfer models (for an overview, see *Bais et al.* [2003]) that use the extraterrestrial solar spectrum as input, as well as vertical distributions of atmospheric parameters (pressure, temperature, aerosol, ozone, clouds) and the Earth's surface albedo. The models also require the absorption and scattering cross sections for the interaction of solar radiation with atmospheric gases and aerosols. In a second step, $j(O^1D)$ is determined according to equation (2), requiring the knowledge of the photodissociation parameters σ and ϕ of reaction (R1).

[6] Despite the important role of $j(O^1D)$ in atmospheric chemistry, only a few studies have been performed to date on how well $j(O^1D)$ can be measured or modeled. In the

Table 1. Experimental Methods and Their Application for the Measurement of $j(O^1D)$ to Date

Reference	Methods[a]	Platform
Bahe and Schurath [1978]	CA	ground and balloon
Bahe et al. [1979]	CA	ground
Dickerson et al. [1979]	CA	ground
Dickerson et al. [1982]	CA	ground and aircraft
Junkermann et al. [1989]	FR and CA	ground
Bairai and Stedman [1992]	CA	ground
Blackburn et al. [1992]	CA	ground
Hofzumahaus et al. [1992]	FR	ground, ship
Junkermann [1994]	FR	hang glider
Müller et al. [1995]	SR and CA	ground
McElroy et al. [1995]	SR	aircraft
Shetter et al. [1996]	CA	ground
Kraus and Hofzumahaus [1998]	SR	ground
Brauers et al. [1998]	FR	ground
Monks et al. [1998]	FR	ground
Hofzumahaus et al. [1999]	SR	ground
Shetter and Müller [1999]	SR	aircraft
Crawford et al. [1999]	SR	aircraft
Pfister et al. [2000]	FR	aircraft
Junkermann [2001]	FR	ultralight aircraft
Lefer et al. [2001]	SR	ground
Hofzumahaus et al. [2002]	SR	aircraft
Shetter et al. [2002]	SR	aircraft
Eckstein et al. [2002]	SR	ground
Kanaya et al. [2003]	SR	ground

[a]CA, chemical actinometry; SR, spectroradiometry; FR, filter radiometry.

first direct intercomparison of $j(O^1D)$ measurement techniques, *Müller et al.* [1995] compared independent measurements obtained by a spectroradiometer and a chemical actinometer and found agreement within the combined experimental errors (14%). *Shetter et al.* [1996] compared results from their chemical actinometer with concurrent measurements by an actinic flux filter radiometer. They reported agreement within 10% at noon but found increasing deviations toward higher SZA of more than 40%, which they attributed to the fixed bandwidth problem of the filter radiometer. *Kraus and Hofzumahaus* [1998] compared spectroradiometer measurements of $j(O^1D)$ with results from a calibrated actinic flux filter radiometer that had been corrected for the fixed bandwidth problem. They found good agreement (within 5%) that persisted even at high SZA [*Brauers et al.*, 1998].

[7] Models have been tested against $j(O^1D)$ measurements on relatively few occasions. In their pioneering work, *Bahe et al.* [1979] and *Dickerson et al.* [1979] applied chemical actinometry and confirmed the general theoretically predicted dependence of $j(O^1D)$ on the vertical ozone column and SZA. *Shetter et al.* [1996] compared model predictions of $j(O^1D)$ with measurements by a chemical actinometer operated on Mauna Loa (Hawaii). They obtained quantitative agreement within 15% for clear-sky conditions. Cloud effects on $j(O^1D)$ were studied by *Crawford et al.* [1999], *Pfister et al.* [2000], and *Junkermann* [2001]. They compared model results with airborne spectroradiometer and filter radiometer measurements.

[8] One model-model comparison for $j(O^1D)$ has been reported by the Intergovernmental Panel on Climate Change (IPCC), which evaluated model differences within the tropospheric photochemical model intercomparison (PhotoComp) in 1994 [*Olson et al.*, 1997]. The $j(O^1D)$ predictions of 21 models were found to scatter around the mean of the model results by 6–9% (root-mean-square) after discarding one obvious outlier. This result was obtained for clear sky and refers to noon values as well as diurnal averages. One suggestion for future work was to perform a closer examination of model-generated diurnal profiles of j values and compare them with measurements.

[9] An important aspect in the determination of $j(O^1D)$ from modeled or measured actinic flux is the accuracy of the photochemical data (σ, ϕ) used for the evaluation of equation (2). Two experimental field studies have been reported to date that investigated the appropriateness of recommended molecular data for the description of $j(O^1D)$ in the atmosphere. In their $j(O^1D)$ comparison between a chemical actinometer and a spectroradiometer, *Müller et al.* [1995] investigated the contribution of $O(^1D)$ formation to $j(O^1D)$ at wavelength above 315 nm, for which controversial quantum yield data existed in the literature. They obtained general agreement when they applied published quantum yield data that exhibited a long-wavelength tail above 315 nm, whereas quantum yield data without such a tail produced significant discrepancies reaching more than 50% at high SZA. This observation supported the existence of the tail, a spectral feature observed in some laboratory studies [*Brock and Watson*, 1980; *Trolier and Wiesenfeld*, 1988; *Ball et al.*, 1993] that were not generally accepted at that time [*DeMore et al.*, 1994]. Further experimental support came from the field study by *Shetter et al.* [1996], who could resolve discrepancies between their chemical actinometer data and modeling results only when they used $O(^1D)$ quantum yields with a tail in their model. Major progress in the understanding of the molecular photodissociation processes of O_3 has been made through theoretical work [*Michelsen et al.*, 1994] and since 1995 through a series of new laboratory studies (for an overview, see *Matsumi et al.* [2002]). The experimental and theoretical efforts have led to a sequence of revisions of the recommendation of the $O(^1D)$ quantum yield [*DeMore et al.*, 1997; *Sander et al.*, 2000, 2003; *Matsumi et al.*, 2002], which have not been tested against field data so far.

[10] In summer 1998, the International Photolysis Measurement and Modeling Intercomparison (IPMMI) Study took place at the Marshall field site near Boulder, Colorado, and offered an outstanding opportunity to test how well current-state experimental techniques and models can determine the solar spectral actinic flux and the photolysis frequencies of ozone ($j(O^1D)$) and nitrogen dioxide ($j(NO_2)$). Eight different research groups participated in a blind intercomparison of measurements using chemical actinometers and radiometers during an intensive of 4 days (15, 16, 18, and 19 June). In a separate but related study, 16 theoretical models by 14 different research groups were compared. The blindly submitted data of the experimental and theoretical studies were first evaluated separately by independent referees before the experimental and theoretical data were exchanged and made available to the participants of IPMMI. An overview of IPMMI and ancillary measurements are given by *Cantrell et al.* [2003]. Related papers present the results of the intercomparisons of the measured and modeled actinic flux [*Bais et al.*, 2003], $j(NO_2)$ [*Shetter et al.*, 2003], and $j(O^1D)$ (this paper). The specific goals of the present paper are to compare the different measurement techniques for $j(O^1D)$ against each other and the theoretical modeling of $j(O^1D)$ against measurements. The comparisons will be made for diurnal profiles including high and low Sun, as well as clear-sky and cloudy conditions. Further, there is a quantitative assessment of the use of different molecular parameters for the derivation of $j(O^1D)$ and an assessment of the role of the temperature dependence of the molecular parameters on the experimental determination of $j(O^1D)$. The paper concludes with an assessment of the issues arising and implications of the work for determination of $j(O^1D)$ by both models and measurements.

2. Experiment

[11] Eleven different instruments were used by six different groups to measure $j(O^1D)$. The instruments included one chemical actinometer, six spectroradiometers, and four filter radiometers. The names of the institutes that operated the instruments are given in Table 2. The techniques, their calibrations, and estimated measurement errors are summarized in Table 3. A short overview of the applied techniques is included below, and brief technical descriptions of individual instruments are given in Appen-

Table 2. Groups Contributing $j(O^1D)$ Data to IPMMI

Institute	Short Name
Measurement Groups	
Forschungszentrum Jülich	FZJ
Institut für Meteorologie und Klimaforschung (former Fraunhofer Institut für Atmosphärische Umweltforschung)	IFU
Meteorologie Consult GmbH	MET
National Center for Atmospheric Research	NCAR
National Institute of Water and Atmospheric Research	NIWA
University of Leicester	ULI
Modeling Groups	
National Center for Atmospheric Research	ACD
Meteorological Service of Canada	AES
British Antarctic Survey	BAS
Institut für Physik der Atmosphäre, DLR	BM1, BM2, BM3
Johns Hopkins University, Applied Physics Laboratory	JHU
Forschungszentrum Jülich	KFA
Karl-Franzens Universität	KFU
Royal Netherlands Meteorological Institute	KNM
Institute for Marine and Atmospheric Research	MAR
Norwegian Institute for Air Research	NIL, NI2
NOAA Aeronomy Laboratory	NOA
Meteorologisches Institut Universität München	UMU

dix A. Additional information is found in the IPMMI introductory paper [*Cantrell et al.*, 2003].

2.1. Instrumental Overview

2.1.1. Chemical Actinometer

[12] This category of instrumentation was represented by one instrument used by NCAR during the IPMMI campaign. The chemical actinometer (CA-NCAR) was similar to the one described in detail by *Shetter et al.* [1996] and is based on the following series of reactions utilized by *Blackburn et al.* [1992] in a similar instrument:

$$\text{(R5)} \qquad O_3 + h\nu \longrightarrow O(^1D) + O_2\left(^1\Delta_g, {}^3\Sigma_g^-\right),$$

$$\text{(R6)} \qquad O(^1D) + N_2O \longrightarrow NO + NO,$$

Table 3. Instruments and Calibration Data Used for the Comparison of Experimental $j(O^1D)$ Data[a]

Method[b]	Technique[c]	Instrument[d]	σ[e]	ϕ[f]	T[g]	Calibration Reference	Error, %		
							Instrument	Other	Total
CA	flow tube	CA-NCAR	–	–	Act	NO standard	5	10[h]	11.2
SR	DM/PMT	SR-FZJ	MM	TAL	Act	lamp (FZJ)	6[i]	10.4[j]	12
SR	DM/PMT	SR-MET1	MM	JPL97	298 K	lamp (NCAR)	–[k]	10.4[j]	–[k]
SR	DM/PMT	SR-NCAR	MM	TAL	Act	lamp (NCAR)	6.6[i]	10.4[j]	12.3
SR	SM/PDA	SR-MET2	MM	JPL97	298 K	SR-MET1	–[k]	10.4[j]	–[k]
SR	SM/PDA	SR-ULI	MM	TAL	Act	lamp (NCAR)	6.5[i,l]	10.4[j]	12.3[l]
SR	SM/PDA	SR-ULI*	MM	TAL	Act	lamp (NCAR)			
SR (Irrad.)	DM/PMT	SR-NIWA	MM	TAL	Act	lamp (NIWA)	6[i]	10.4[j]	–[k]
FR	filter/PMT	FR-FZJ	MAL	TAL	298 K	lamp (FZJ)	6[m]	11.7[j,n]	13.2
FR	filter/PMT	FR-FZJ*	MAL	TAL	Act	lamp (FZJ)			
FR	filter/PMT	FR-IFU	MM	JPL94	298 K	CA-IFU	12[m]	9[j,n]	15
FR	filter/PMT	FR-IFU*	MM	JPL94	298 K	CA-IFU			
FR	filter/PMT	FR-MET	MAL	BW	298 K	SR-MET1	–[k]	–[k]	20
FR	filter/PMT	FR-ULI	MM	JPL97	298 K	CA-FZJ	–[k]	10.4[j]	12

[a]The specified errors are associated with the originally submitted j values.
[b]CA, chemical actinometry; SR, spectroradiometry; FR, filter radiometry.
[c]SM, single monochromator; DM, double monochromator; PMT, photomultiplier tube; PDA, photodiode array.
[d]Identifier of the instrument and the operating group. An asterisk denotes that the respective $j(O^1D)$ data set was revised after the blind phase of the intercomparison (see text).
[e]Ozone absorption spectrum: MM, *Molina and Molina* [1986]; MAL, *Malicet et al.* [1995].
[f]$O(^1D)$ quantum yield: TAL, *Talukdar et al.* [1998]; BW, *Brock and Watson* [1980]; JPL94, *DeMore et al.* [1994]; JPL97, *DeMore et al.* [1997].
[g]Temperature for which $j(O^1D)(T)$ was evaluated; Act denotes the temperature of the instrument CA-NCAR.
[h]Associated with the branching ratio of the $N_2O + O(^1D)$ reactions in the chemical actinometer.
[i]Associated with the radiation calibration, wavelength accuracy, spectral bandwidth, and stray light rejection.
[j]Associated with O_3 absorption cross section (3%) and $O(^1D)$ quantum yield (10%).
[k]Not specified.
[l]Errors due to stray light not included.
[m]Associated with the absolute calibration.
[n]Associated with T, SZA, and O_3 column corrections to filter radiometer signals.

(R7) $$O(^1D) + N_2O \longrightarrow N_2 + O_2,$$

(R8) $$NO + O_3 \longrightarrow NO_2 + O_2,$$

(R9) $$NO_2 + O_3 \longrightarrow NO_3 + O_2,$$

(R10) $$NO_3 + NO_2 + M \longrightarrow N_2O_5 + M,$$

(R11) $$N_2O_5 + H_2O(l) \longrightarrow 2\ HNO_3(l).$$

The primary reaction of $O(^1D)$ is the reaction with N_2O yielding either N_2 or O_2 via reaction (R6) or NO via reaction (R5). In the ozone-rich environment in the instrument, the NO produced by reaction (R5) produces NO_2, the NO_2 is then converted to NO_3, and further on to gas phase N_2O_5, which is readily converted to HNO_3 upon contact with liquid water. The NO_3^- is then detected by conductivity.

2.1.2. Spectroradiometers

[13] This category of instrumentation was represented by six radiometers, for which short descriptions can be found in Appendix A1. Five of the instruments were used to measure the downwelling actinic flux from which $j(O^1D)$ values were calculated. Each instrument independently collected the radiation through tower mounted (~5 m) 2π steradian (sr) light collecting optics. Three of the systems (SR-FZJ, SR-MET1, SR-NCAR) used serially scanning double-monochromators and photomultipliers for the actinic flux measurements. Two other instruments (SR-MET2, SR-ULI) employed a single-monochromator photodiode-array assembly to measure in parallel the full wavelength range. Photolysis frequencies were then directly calculated from each of the measured actinic fluxes. Another sequentially scanning double-monochromator system (SR-NIWA) used a cosine-weighting entrance optic to measure the solar irradiance. The irradiance spectra were used instead of actinic flux spectra to calculate pseudo $j(O^1D)$ values [*McKenzie et al.*, 2002].

2.1.3. Filter Radiometers

[14] This category of instrumentation was represented by four radiometers (FR-FZJ, FR-MET, FR-IFU, and FR-ULI) for which brief descriptions are given in Appendix A2. The instruments originate from the concept of *Junkermann et al.* [1989] and included technical modifications that improve the performance of the instruments. Two instruments (FR-FZJ and FR-MET) were from the same commercial manufacturer, whereas the two other radiometers (FR-IFU, FR-ULI) were homemade. The four filter radiometers collected the downwelling 2π sr actinic flux at 5 m height. They used fixed combinations of optical filters and electrical photodetectors to measure the broad-band integrated radiation responsible for $O(^1D)$ formation from ozone photolysis. The raw signals were then converted into $j(O^1D)$ by means of individual calibration functions.

2.2. Calibrations of $j(O^1D)$ Measurements

[15] The most relevant calibration parameters of the individual instruments are summarized in Table 3. It should be noted that some instruments used identical calibration references. This procedure removes bias that otherwise could possibly result from the use of different calibration standards. On the other hand not all radiometer evaluations used the same molecular data (σ, ϕ). As discussed later, this introduces a priori differences in the calculated $j(O^1D)$ values, even if the instruments agree in their radiation measurements. Some more comments specific to the different measurement methods are given in the following.

2.2.1. Chemical Actinometer

[16] Chemical actinometry has the inherent advantage that its calibration is independent of the knowledge of σ and ϕ and accounts naturally for the temperature dependence of $j(O^1D)$. For these reasons it is a very useful reference for comparisons with radiometers that rely on the correct data for $\sigma(\lambda, T)$ and $\phi(\lambda, T)$. It must be noted, however, that during IPMMI the gas temperature (*T-Act*) inside the chemical actinometer (CA-NCAR) was often above ambient air temperature. The elevated temperature was due to insolation that heated the black surface installed beneath the actinometer flow tube. The reason for the black surface was to shield the actinometer against upwelling actinic radiation reflected from the ground and from the sea container on which the actinometer had been mounted.

2.2.2. Spectroradiometers

[17] All spectroradiometers were calibrated against irradiance standards of the same type (FEL 1000 W quartz-tungsten-halogen lamps), but were traceable to different national standards (FZJ lamp: PTB; NCAR and NIWA lamps: NIST). Note that SR-MET1 and SR-ULI used the NCAR lamp for calibration and are therefore not independent in their absolute calibrations of radiation. Also note that the absolute calibration of SR-MET2 was obtained by comparison with SR-MET1.

[18] Each spectroradiometer was expected to provide $j(O^1D)$ values for different combinations of molecular parameters and temperatures that were prescribed by the IPMMI data protocol for the measurements [*Cantrell et al.*, 2003]. For the absorption cross section $\sigma(\lambda, T)$ the data by *Molina and Molina* [1986] were to be used, while two sets of data were prescribed for the quantum yield $\phi(\lambda, T)$: the recommendation by *DeMore et al.* [1997] (hereinafter referred to as JPL97) and the measurements by *Talukdar et al.* [1998] (hereinafter referred to as TAL) that had been published shortly before the IPMMI campaign. Furthermore the measured temperatures of the ambient air and of the chemical actinometer were made available by the referee after the campaign. Note that the SR-MET1 and SR-MET2 data were submitted for only one quantum yield (JPL97 at 298 K).

2.2.3. Filter Radiometers

[19] For the absolute calibration of the filter radiometers each group used a different reference. The calibrations of FR-IFU and FR-ULI are traceable to previous comparisons with chemical actinometers. The FZJ filter radiometer was calibrated against the irradiance standard which was also used for the FZJ spectroradiometer. The FR-MET calibration was obtained by scaling the $j(O^1D)$ data against the corresponding SR-MET1 measurements.

[20] Furthermore, each group used its own evaluation procedure to account for nonlinearities in the relationship between $j(O^1D)$ and the measurement signals. The nonlinearities depend mainly on SZA, overhead O_3 column, and the temperature that directly affects $j(O^1D)$. SZA values

were calculated by each group from the known geographical position and the time of measurements, and measurements of the overhead O_3 column and the diurnal temperatures were provided by the referee. Moreover, the $j(O^1D)$ evaluation requires molecular data for σ and ϕ for which the groups used different data sets (Table 3).

[21] The FR data blindly submitted by each group apply to a constant temperature of 298 K and thus, neglect the natural temperature dependence of $j(O^1D)$. Only in a revised version of the FR-FZJ data is the $j(O^1D)$ temperature effect taken into account (see below).

2.3. Estimated $j(O^1D)$ Measurement Errors

[22] It is important to appreciate the errors (Table 3) associated with the different $j(O^1D)$ measurements when comparing the reported IPMMI results. The overall error is a combination of the instrument error (e.g., calibration, light collection, etc.) and other errors not related to the operation of the instrument but included in the final reported $j(O^1D)$ value. The overall error for all of the measurements is on the order of 12–20%. The uncertainty in the N_2O branching ratio (10%) is the largest source of uncertainty for the chemical actinometer. For the spectroradiometers the 12% error is primarily due to the estimated 10% uncertainty in the quantum yield data. No total $j(O^1D)$ error is specified for the NIWA instrument, because it calculated pseudo $j(O^1D)$ values from irradiances rather than j values from actinic fluxes. The filter radiometer errors are more evenly distributed between calibration errors and the uncertainty due to the conversion equation, which incorporates temperature, solar zenith angle, and overhead O_3 column.

[23] In two cases, data submitted to the referee were tagged as "may be a problem." One case was the FR-ULI data for 19 June between 1637 and 1659 MDT. During this time period the temperature stabilization of the filter radiometer lost control because of high ambient temperatures, which possibly affected the calibration of the instrument. The second case was the FZJ spectroradiometer data submitted for 16 June as some condensation of water was observed in the entrance optic. On the evening of 16 June the head was removed, dried, and a new field calibration of the spectroradiometer was made on 17 June. Study of this potential problem after data submission suggested that moisture may have entered during the evening of 14 June and been present during measurements on 15 and 16 June; hence data for these days is considered to be of uncertain accuracy. After drying and reassembly of the collector head, stable calibrations were obtained on the following days: 17–20 June.

3. Comparison of Experimental Data

[24] All $j(O^1D)$ instruments were operated simultaneously on four measurement days (15, 16, 18, and 19 June 1998) on the Marshall field site near Boulder, Colorado. The general measurement conditions are summarized in Table 4, and details can be found in the IPMMI overview paper by *Cantrell et al.* [2003]. Each instrument measured $j(O^1D)$ contributed by the downwelling actinic flux (2π sr) at a height of ~5 m above ground which had a small albedo of 2–3%. The measurements were carried out continuously from 0500 to 2100 MDT each day. Each group averaged and assigned their $j(O^1D)$ measurements to prescribed time grids of 1-, 10-, and 30-min time resolution, of which the 1-min-averaged data will be reported in this paper. On the first three measurement days (15, 16, and 18 June) the sky was cloudy, whereas the 19 June was a day with clear sky. The ambient temperatures ranged from a minimum of 5°C (15 June, 0535 MDT) to a maximum of 33°C (19 June, 1735 MDT). The temperature of the $j(O^1D)$ actinometer was the same as of ambient air at night, but was higher because of insolation during the day and reached a maximum of 45°C (19 June, 1545 MDT). The minimum solar zenith angle was 16.5° (1304 MDT, local noon) and total O_3 columns were between 307 and 349 Dobson Units (DU).

Table 4. General Conditions of the $j(O^1D)$ Intercomparison During IPMMI[a]

Parameter	Value
Field site	Marshall field, Boulder, Colorado
Geographic position	39°57′N, 105°12′W, 1800 m ASL
Measurement height	~5 m
Viewing angle	2π steradian (upper hemisphere)
Measurement days	15, 16, 18, and 19 June 1998
Measurement times	0500–2100 MDT[b]
Minimum solar zenith angle	16.5°
Temperatures	see Figure 2
Clouds/total ozone[c]	15 June: broken clouds/349 DU
	16 June: broken clouds/335 DU
	18 June: broken clouds/335 DU[d]
	19 June: clear sky/307 DU
Aerosol optical depth	19 June: 0.03 ± 0.02 at 550 nm
Albedo	0.026–0.029

[a]For details, see *Cantrell et al.* [2003].
[b]Mountain Daylight Time.
[c]Total vertical ozone columns at noontime, measured by the NOAA Dobson spectrometer about 8 km northwest of the IPMMI site.
[d]Mean value of 327 DU at 1000 MDT and 343 DU at 1400 MDT.

3.1. Diurnal Profiles

[25] The blind $j(O^1D)$ data measured by the actinic flux spectroradiometers and filter radiometers are presented in Figure 2 for an overview. The plots of the diurnal profiles are arranged in a matrix where each column represents one measurement day and each row displays the measurements of one instrument. In each $j(O^1D)$ plot the corresponding diurnal variations of the chemical actinometer (CA-NCAR) are shown for comparison. The temperatures of the chemical actinometer and of ambient air are displayed in the lowest panels of Figure 2a.

3.1.1. SR Versus CA

[26] For a meaningful comparison, the spectroradiometer data (Figure 2a) were chosen, where possible, for the same set of input parameters, namely the absorption cross sections by *Molina and Molina* [1986] and the quantum yield by *Talukdar et al.* [1998]. Moreover, the temperature (*T-act*) measured inside the chemical actinometer was chosen to enable a direct comparison to the CA instrument. An exception are the $j(O^1D)$ data by SR-MET1 and SR-MET2 which were submitted only for the quantum yield JPL97 [*DeMore et al.*, 1997] at 298 K.

[27] In general, all instruments measured similar diurnal profiles. On the cloud-free day, 19 June, the profiles look smooth as is expected for such conditions. On the days 15, 16, and 18 June, fast fluctuations can be seen due to varying broken clouds. A closer look reveals some differences

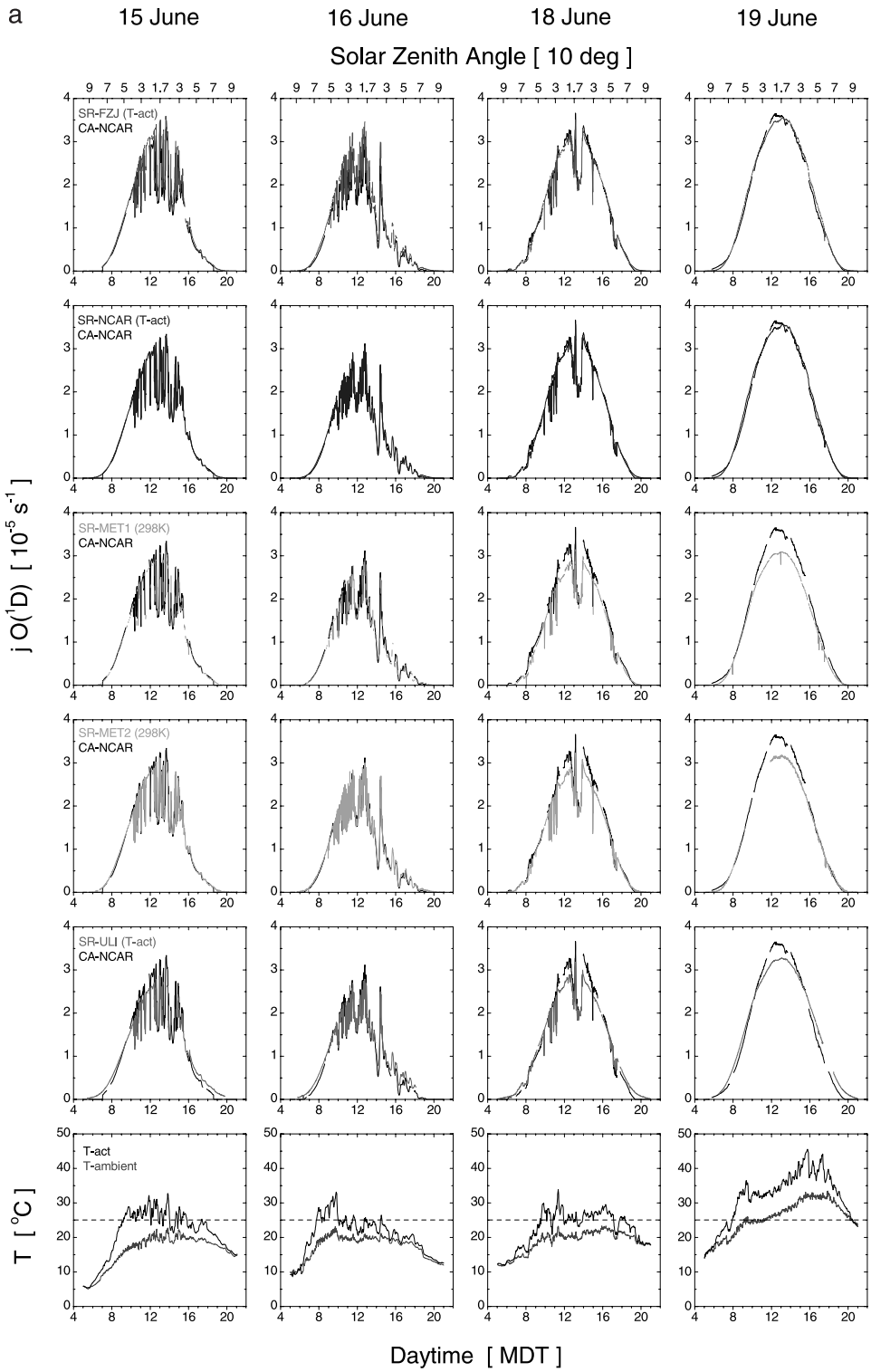

Figure 2. Diurnal profiles of 1-min data of $j(O^1D)$ and temperatures during IPMMI. (a) Comparison of actinic flux spectroradiometers with the chemical actinometer (CA-NCAR). The spectroradiometer data use the ozone absorption cross section $\sigma(\lambda, T)$ from *Molina and Molina* [1986], the quantum yield $\phi(\lambda, T)$ by *Talukdar et al.* [1998], and the temperature of the chemical actinometer. SR-MET1 and SR-MET2 use the quantum yield by *DeMore et al.* [1997] and assume a fixed temperature (298 K) for σ and ϕ. The lowest panel shows measured temperatures of the chemical actinometer and of ambient air. The dashed horizontal line denotes 298 K. (b) Comparison of filter radiometers with the CA-NCAR instrument. All FR data apply to 298 K. Other parameters used for the evaluation of the FR data are given in Table 3. See color version of this figure at back of this issue.

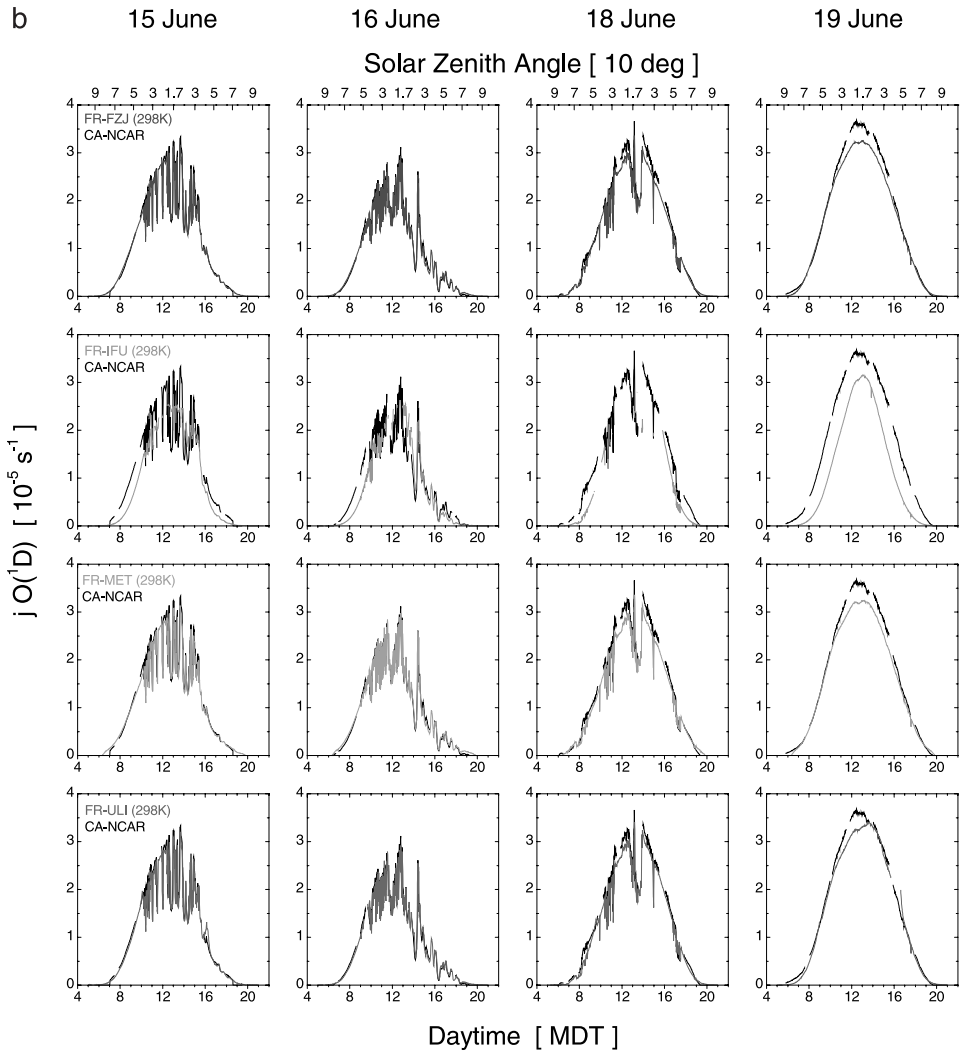

Figure 2. (continued)

between the data of different instruments, like the noontime data on 19 June. The smoothness of the curves on this day indicates that all instruments had a very high measurement precision and most of the differences seen between two instruments are due to systematic measurement errors of one or the other instrument. The most notable features in the comparison of the diurnal $j(O^1D)$ profiles in Figure 2a can be summarized as follows.

[28] For SR-FZJ and SR-NCAR the measurements of these two instruments show a similar behavior and agree excellently with the CA-NCAR data for most of the time, although some systematic temporary deviations can be recognized. For example, both spectroradiometers show the same systematic deviation of +4% relative the CA readings on 19 June at 1230 MDT. Another significant difference is apparent at sunrise on the same day when the CA signal starts to rise earlier than the spectroradiometers readings.

[29] For SR-MET1 and SR-MET2 the diurnal $j(O^1D)$ profiles by these instruments show very similar features. For example, they agree well with the chemical actinometer on the days 15 and 16 June, whereas they show noontime maxima that are 10–15% lower than the data of the CA-NCAR, SR-FZJ, and SR-NCAR instruments on the days 18 and 19 June. The similarity between the SR-MET1 and SR-MET2 data is consistent with their common calibration. Both instruments used the same molecular input data ($\sigma(298\ K)$, $\phi(298\ K)$), and the absolute calibration of SR-MET2 was obtained by scaling its readings to the absolutely calibrated SR-MET1 data.

[30] For SR-ULI the measurements of this instrument show some pronounced systematic deviations from the chemical actinometer data as is evident in the shape of the diurnal profiles. At noon of the days 15, 18, and 19 June the SR-ULI data are roughly 10% lower than the measurements of the chemical actinometer. In contrast, the SR-ULI data are systematically higher than the CA-NCAR measurements in the early morning and late afternoon on all days, with increasing overpredictions at higher solar zenith angles. The reason for this behavior has been identified by the ULI group as an insufficiently corrected background signal that was caused by internal monochromator straylight (see revised data section below and *Edwards and Monks* [2003]).

3.1.2. FR Versus CA

[31] The measurements by the actinic flux filter radiometers are compared to the chemical actinometer data in

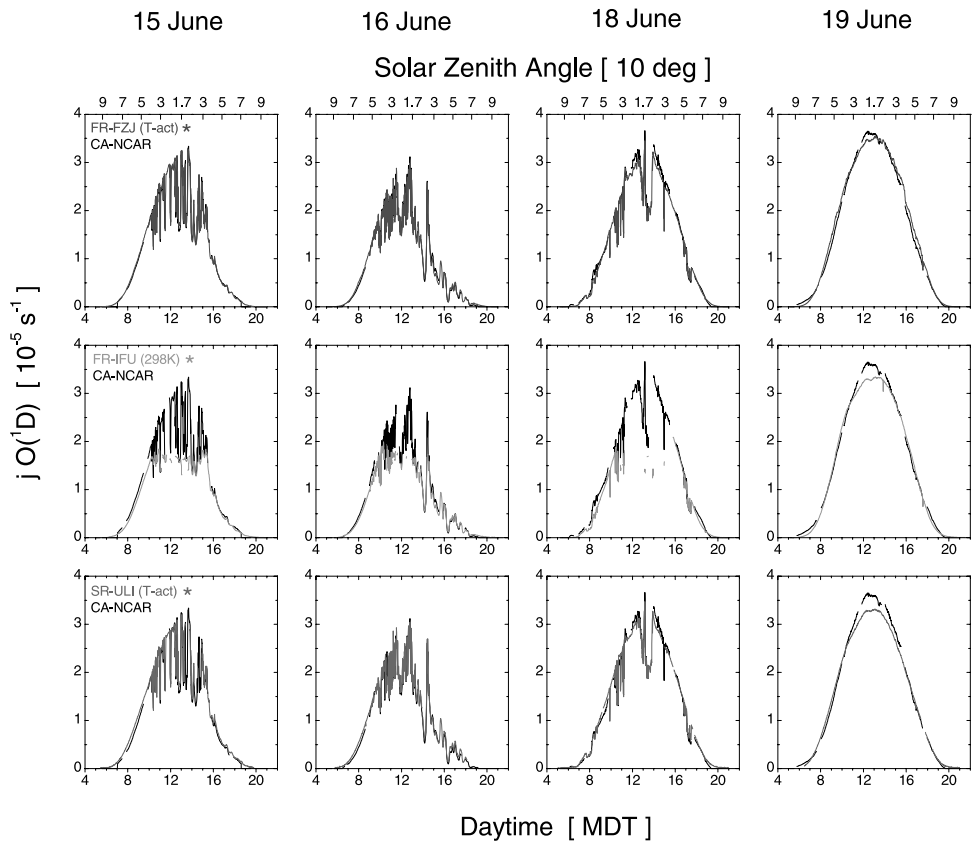

Figure 3. Revised 1-min data of $j(O^1D)$ measured by the instruments FR-FZJ, FR-IFU, and SR-ULI. The revised data, marked with an asterisk, are explained in the text. FR-FZJ* and SR-ULI* use the temperature of the chemical actinometer, whereas FR-IFU* uses 298 K for the evaluation of $j(O^1D)$. The CA-NCAR data are the same as in Figure 2. See color version of this figure at back of this issue.

Figure 2b. Note that all FR data were provided for a constant temperature of 298 K only, whereas the j values by the CA-NCAR instrument are temperature dependent. The main features of the comparison can be described as follows.

[32] The FR-FZJ, FR-MET, and FR-ULI instruments recorded diurnal profiles of $j(O^1D)$ that look very similar. The FR data show quite good agreement with the chemical actinometer results on the first two measurement days (15 and 16 June), but are about 5–10% lower than the CA-NCAR measurements during the noon of 18 and 19 June. A similar behavior is found in the diurnal profiles of SR-MET1 and SR-MET2 in Figure 2a. The $j(O^1D)$ values of the instruments FR-FZJ, FR-MET, FR-ULI, SR-MET1, and SR-MET2 have in common that they were evaluated for a fixed temperature of 298 K. The missing temperature dependence can explain much of the deviations from the chemical actinometer measurements as will be shown below. The temporary enhancement of the FR-ULI data on 19 June between 1637 and 1659 MDT can be explained by the malfunction of the temperature stabilization of the instrument as was tagged in the submitted data for this time interval.

[33] The photolysis frequencies of the FR-IFU radiometer deviate strongly from the results of all other instruments. The most pronounced discrepancy is seen in the width of the diurnal profiles which are much narrower than observed by the chemical actinometer. The reason for this behavior has been identified by the IFU group as a faulty conversion of the radiometer signals into $j(O^1D)$ values (see revised data in the next section).

3.2. Revised Diurnal Profiles

[34] The blindly submitted data were first analyzed by the referee before they were made available to all experimental groups. Thereafter, deviations observed between measurements of different instruments were investigated by the participants. In some cases, systematic errors were identified and corrected. Three groups resubmitted new data after the blind phase. The revised data are presented in Figure 3 and are marked by the asterisk symbol appended to the instrument's name (e.g., FR-FZJ*) to distinguish them from blindly submitted data. The groups gave the following explanations of the changes made to their data.

[35] For FR-FZJ a parametrization of the temperature dependence of $j(O^1D)$ has been developed [*Bohn et al.*, 2004] and was applied to convert the originally submitted data valid for 298 K into temperature-dependent j data. The parametrization represents the ratio $j(O^1D)(T)/j(O^1D)(298K)$, where $j(O^1D)$ is simulated by modeled actinic flux spectra for a range of solar zenith angles (0°–80°) and total O_3 columns (240–460 DU). The simulation uses the temperature-dependent ozone absorption cross section by *Malicet et al.* [1995] and the quantum yield by *Talukdar et al.* [1998]. The modeled ratio

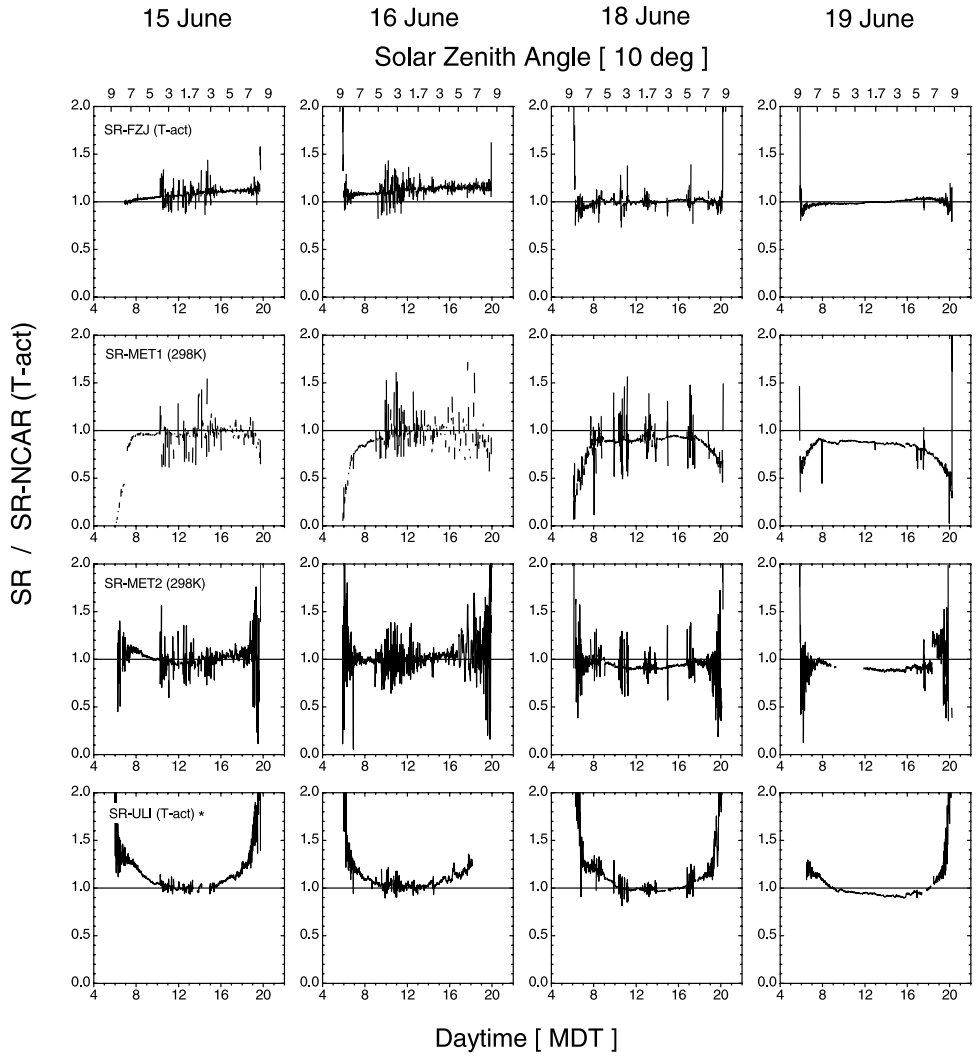

Figure 4. Ratios of 1-min data of $j(O^1D)$ measured by the various radiometers relative to the SR-NCAR instrument. The data of the radiometers were evaluated using the parameters $\sigma(\lambda, T)$ and $\phi(\lambda, T)$ as explained in the captions of Figures 2 and 3. In the case of SR-ULI and FR-IFU only the revised data are considered. Solid horizontal lines indicate a ratio of 1.

$j(O^1D)(T)/j(O^1D)(298\ K)$ was then parameterized as a function of solar zenith angle and overhead O_3 column and applied to the original $j(O^1D)(298\ K)$ filter radiometer measurements for the conditions of IPMMI in order to generate revised FR data.

[36] For FR-IFU the IPMMI data files for $j(O^1D)$ were revised after a calculation error was found in the original files. The original files were generated using a correction data set for the overhead O_3 column density based on a STAR model calculation with improper spacing of wavelength intervals. Additionally the correction applied was done with a division instead of a multiplication with the effective O_3 column correction function. Thus the diurnal curve gets narrower instead of broader compared to the original filter radiometer raw data. The revised data set was calculated with a new correction curve based on a revised calculation using the latest version of the STAR model and a proper wavelength spacing and with the correction function applied in the right way.

[37] For SR-ULI the problem of poor instrument stray light rejection in the single-monochromator photodiode-array spectroradiometer deployed by the University of Leicester at IPMMI has implications for the accuracy of the derived photolysis frequencies. The original $j(O^1D)$ data were evaluated from actinic flux spectra that were in situ corrected for stray light by subtracting a wavelength-independent offset calculated as the average of the spectroradiometer signals between 285 nm and 290 nm. In order to improve the data further following the conclusion of the IPMMI experiment an actual stray-light spectrum with respect to wavelength was measured on a cloud-free day at the University of Leicester [*Edwards and Monks*, 2003]. The revised $j(O^1D)$ data were obtained after application of the wavelength-dependent stray-light spectrum in the correction of the spectral data recorded at IPMMI.

3.2.1. Revised Radiometers Versus CA

[38] For FR-FZJ the revised filter radiometer data FR-FZJ* agree much better with the measurements of the

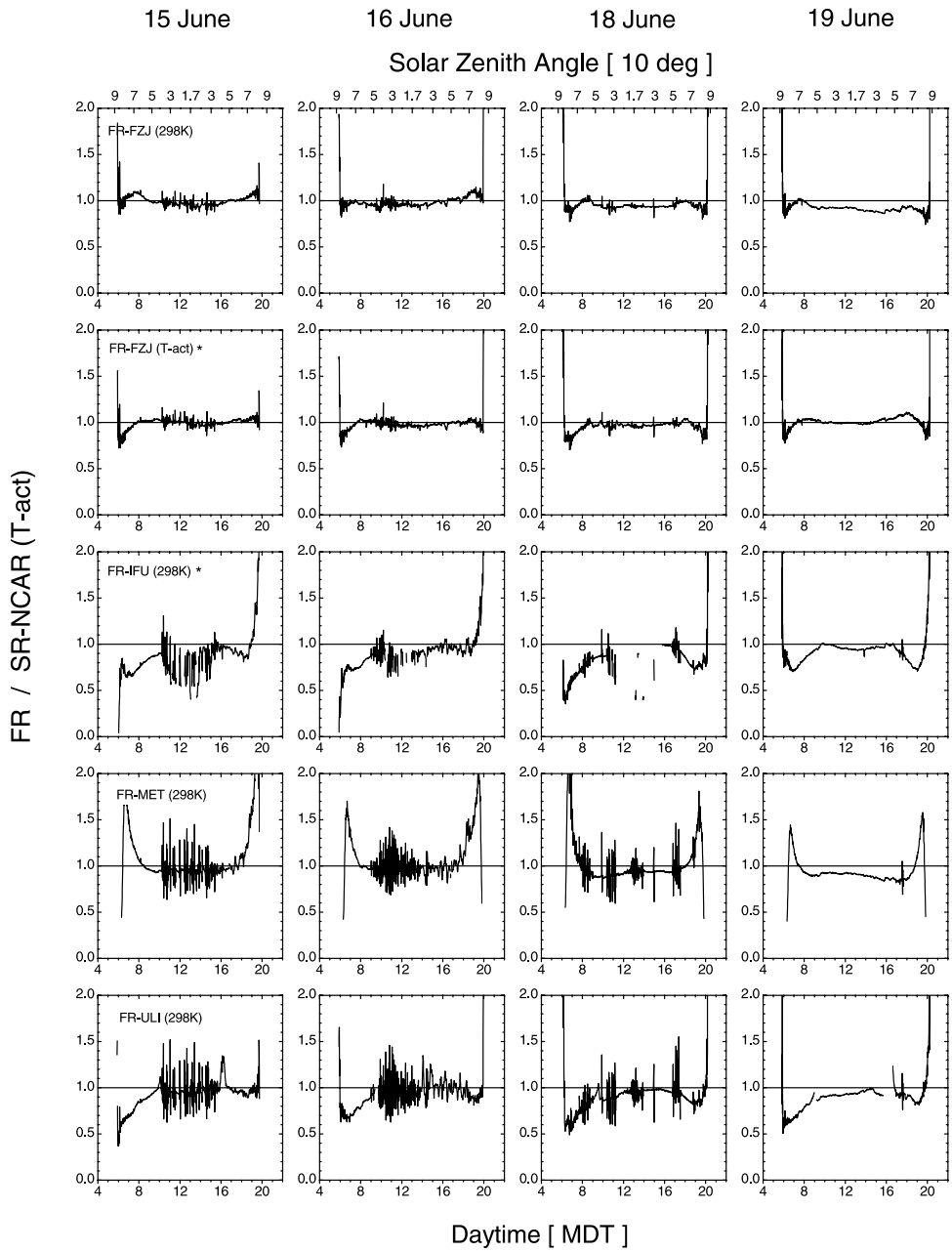

Figure 4. (continued)

chemical actinometer (Figure 3) than is the case for the uncorrected data (compare Figure 2b). In particular, the underprediction of $j(O^1D)$ by the uncorrected filter radiometer data found during noon of 18 and 19 June is mostly removed. This leads to the same excellent agreement with the chemical actinometer as is observed for the spectroradiometers SR-FZJ and SR-NCAR (Figure 2a) which explicitly consider the temperature influence on the ozone photolysis.

[39] For FR-IFU the revised FR-IFU* data (Figure 3) are in much better agreement with the j values of the chemical actinometer than the original data. In particular, the width of the diurnal profiles is now in good agreement with the observations by the other instruments. However, some deviations relative to the CA-NCAR profiles remain, some of which can be explained by the fixed temperature (298 K) used in the reevaluation of the filter radiometer data.

[40] For SR-ULI the new stray light correction of the SR-ULI* data improves significantly the agreement with the CA-NCAR measurements. The overprediction of $j(O^1D)$ at sunrise and sunset has greatly diminished and the noon time values are now in good agreement with the CA-NCAR data on the days 15, 16, and 18 June. The systematic deviation around noon of 19 June, however, has not notably changed.

3.3. Ratios of Diurnal Profiles

[41] A more detailed comparison of the radiometer data (Figure 4 and Table 5) is achieved by examining the ratios of the diurnal $j(O^1D)$ profiles versus the measurements by the NCAR spectroradiometer (SR-NCAR). Here, the NCAR

Table 5. Mean Ratios of 1-min Data of $j(O^1D)$ Measured by the Various Radiometers Relative to the SR-NCAR Instrument for Two Ranges of Solar Zenith Angle on the Four Measurement Days[a]

	SZA ≤ 60°				60° < SZA ≤ 85°			
Group	15	16	18	19	15	16	18	19
SR-FZJ	1.08(0.06)	1.13(0.07)	1.00(0.05)	1.00(0.02)	1.08(0.08)	1.12(0.05)	1.01(0.23)	0.99(0.04)
SR-MET1	0.98(0.15)	0.99(0.16)	0.92(0.12)	0.86(0.03)	0.80(0.30)	0.83(0.22)	0.73(0.19)	0.76(0.11)
SR-MET2	1.00(0.08)	1.01(0.11)	0.93(0.08)	0.90(0.03)	1.09(0.37)	1.05(0.25)	0.97(0.28)	0.97(0.21)
SR-ULI*	1.05(0.05)	1.06(0.06)	1.02(0.07)	0.95(0.03)	1.40(0.35)	1.24(0.21)	1.47(0.89)	1.16(0.17)
FR-FZJ	0.97(0.03)	0.97(0.03)	0.95(0.03)	0.91(0.02)	1.06(0.14)	1.01(0.06)	0.98(0.23)	0.93(0.05)
FR-FZJ*	1.00(0.03)	0.98(0.03)	0.97(0.02)	1.01(0.03)	0.98(0.08)	0.97(0.06)	0.95(0.21)	1.00(0.07)
FR-IFU*	0.84(0.14)	0.92(0.07)	0.88(0.13)	0.96(0.03)	0.92(0.55)	0.89(0.22)	0.71(0.12)	0.81(0.08)
FR-MET	0.96(0.09)	0.98(0.09)	0.93(0.08)	0.89(0.03)	1.37(0.38)	1.29(0.30)	1.24(0.38)	1.04(0.21)
FR-ULI	0.98(0.11)	0.98(0.12)	0.94(0.10)	0.93(0.05)	0.85(0.18)	0.83(0.11)	0.81(0.24)	0.80(0.11)

[a]The data in parentheses are the standard deviations of the ratios in the range of corresponding solar zenith angles.

instrument serves as a reference representing the group of data (SR-FZJ, SR-NCAR, FR-FZJ*) which explicitly consider the temperature dependence of $j(O^1D)$ and show excellent agreement with the measurements of the chemical actinometer (see previous section). It is assumed that the good agreement in this group of instruments, which rely on three different methods (CA, SR, FR), is not by chance but demonstrates approximate correctness of the measured $j(O^1D)$ values. Here, unlike in Figure 2, the chemical actinometer is not selected as the reference for two reasons. First, the radiometers have a lower limit of detection than the chemical actinometer. Thus ratioing versus a radiometer yields a better precision at high solar zenith angles (>75°). Second, the comparison of the radiometers among each other is useful in order to examine first how well the instruments agree in their actinic flux calibrations, provided that they use similar data for σ and ϕ. In a second step (section 4) the absolute nature of the radiometer data and their dependence on σ and ϕ is investigated by comparison against the chemical actinometer.

[42] The ratios of the radiometer data versus daytime are shown in Figure 4, where the SR-NCAR data are used as a reference in all cases. An additional scale of solar zenith angles is given at the top of the upper panels. The following discussion will be restricted to the time interval from 0600 MDT to 2000 MDT at SZA < 86° where the detection noise of the radiometers is very small. Only in the case of the single-monochromator diode-array instruments (SR-MET2, SR-ULI) the signal to noise ratio becomes appreciable when the solar zenith angle exceeds 75°.

[43] In the course of the days irregular spikes are apparent in the ratio plots. These spikes are caused by the differing instrumental time response to fast cloud driven modulations in $j(O^1D)$, which occur mostly on days 15, 16, and 18 June. Relatively small spikes (<15%) are observed for the instruments SR-NCAR, SR-ULI*, and FR-FZJ* which measure the actinic radiation evenly during the prescribed 1-min averaging intervals and are synchronized to GPS-time. Slightly larger spikes (<35%) are found for SR-FZJ. This instrument was synchronized to the same time base, but collected the radiation only in a relative short time window (12 s) within the 1-min time interval. The other instruments (SR-MET1, SR-MET2, FR-MET, FR-IFU*, FR-ULI) show even larger spikes up to 50%, which are presumably due to a poor time synchronization.

[44] The two spectroradiometers by FZJ and NCAR and the filter radiometer FR-FZJ* show almost constant ratios (SR-FZJ/SR-NCAR, FR-FZJ*/SR-NCAR) throughout the entire study, indicating that the radiometers measured very similar diurnal variations. The ratios are close to one, which means also good absolute agreement. The deviations from unity are mostly less than 5% (Table 5) which is smaller than the combined calibration errors of the actinic flux measurements. Slightly larger discrepancies of 8% and 12–13% exist between SR-FZJ and SR-NCAR on 15 and 16 June, respectively. While the value of 8% is still consistent with the specified instrumental errors (6% for each instrument), 12–13% is regarded to be a significant deviation. The comparison with the measurements made by the filter radiometer FR-FZJ* suggests that the FZJ spectroradiometer is responsible for the elevated ratios on 15 and 16 June. In fact, the FZJ spectroradiometer data submitted for 16 June were tagged with a ''may be a problem'' flag, as some condensation of water was observed in the 2π sr hemispheric collector head. Liquid droplets in contact with the frosted quartz surfaces inside the collection head increase the optical transmissivity, which can explain the enhanced signals of the FZJ spectroradiometer. It is likely that this problem already existed on 15 June. On the evening of 16 June the head was removed and dried overnight. The following field calibrations (17–20 June) were found to be reproducible within 2%.

[45] Most other instruments show an approximately constant ratio only for solar zenith angles below 60°. Under these conditions very good agreement is observed between the ULI spectroradiometer and the reference instrument. The deviations are in the range of 5% and can be explained by the instrumental calibration errors. In case of the radiometers SR-MET1, SR-MET2, FR-FZJ, FR-MET, and FR-ULI, a particular behavioral pattern is apparent at SZA < 60°. On 15 and 16 June the measurements agree very well, mostly within 1–2%, with the reference (compare Table 5). On 18 June the measurements are slightly lower than the reference by 5–8% and are significantly lower on the warmest day (19 June) by 9–14%. The observed pattern can be explained quantitatively by the temperature dependence of $j(O^1D)$, which is taken into account by SR-NCAR, but is missing in the data evaluation of the mentioned group of instruments. The effect of the temperature on $j(O^1D)$ is on the order of 1% K^{-1} and is directly visible as the difference between the ratio plots of the corrected and uncorrected FZJ filter radiometer data, FR-FZJ*(T) and FR-FZJ(298 K), respectively. If the temperature corrections were applied to SR-MET1, SR-MET2, FR-MET, and FR-ULI, the data of these instruments would also be in excellent agreement with the reference instrument on all four measurement days at

SZA < 60°. This means that aside of the temperature effect the absolute calibrations of these instruments agree with the reference within the specified errors given in Table 3.

[46] In case of the filter radiometer FR-IFU*, the ratio plots show irregular deviations even at SZA < 60°. The behavior is not well represented by the constant calibration error of 12% and cannot be explained by the missing temperature dependence of $j(O^1D)$. The irregular deviations are not observed for any other instrument and point to an unstable sensitivity of the IFU filter radiometer.

[47] Besides calibration errors, $j(O^1D)$ measurements can be subject to systematic errors that correlate with daytime or solar zenith angle. Such errors become apparent as trends in the ratio plots in Figure 4. Possible reasons are potentially manifold, e.g., (1) anisotropic response of the 2π sr hemispheric collector head. (2) nonlinearity of the radiation detection. (3) temperature dependence of optical or electronic components influencing the detection sensitivity of the instrument. (4) internal stray light in monochromators [cf. *Edwards and Monks*, 2003]. (5) imperfect match of the spectral filter-radiometer response to the $O_3 \rightarrow O(^1D)$ photodissociation spectrum $\sigma\phi$ [cf. *Bohn et al.*, 2004].

[48] In case of the spectroradiometers by FZJ and NCAR a weak trend can be seen in the ratio which steadily increases by 4–8% from 0600 to 2000 MDT. The trend is not correlated with solar zenith angle, spectroradiometer signal intensity, or ambient temperature. Moreover, both spectroradiometers were temperature stabilized. Thus most of the above reasons can be excluded. It is conceivable that one or both instruments suffered from some anisotropic azimuthal dependence of the collector head which may explain some of the diurnal trend in the FZJ/NCAR ratio [*Bais et al.*, 2003].

[49] In the range of medium to high solar zenith angles (60° < SZA < 85°) most other radiometers exhibit significant trends in their ratio plots which vary between 0.5 and 2. For example, SR-MET1 shows a strong downward trend at high solar zenith angles that is nearly symmetric with respect to local noon. This significant feature is much larger than the effect of the missing $j(O^1D)$ temperature dependence. Possible reasons could be problems with the solar zenith angle dependence of the collector head or a nonlinearity of the radiation detection system. SR-MET2 exhibits relatively small systematic deviations at high solar zenith angles. The deviations can be partly explained by the missing $j(O^1D)$ temperature dependence. In case of the ULI spectroradiometer SR-ULI* the data show a strong upward trend at SZA > 60°. The reason is most likely an incomplete correction of the signal contribution that is due to internal stray light in the single-monochromator [*Edwards and Monks*, 2003].

[50] The filter radiometers show very different behaviors at solar zenith angles between 60° and 85°. While the filter radiometer FR-FZJ* deviates very little from the reference, other instruments (FR-IFU*, FR-MET, FR-ULI) show significant upward or downward trends. FR-MET and FR-FZJ* have the same technical design, but used different home made calibration functions that convert the voltage signals into $j(O^1D)$ data and correct for the imperfect spectral match of the radiometer response. It is likely that the instrument-specific corrections, which can typically reach a factor of two at high solar zenith angles, were not sufficiently accurate for the FR-MET instrument. In case of FR-IFU* and FR-ULI the deviations from the reference are asymmetric with respect to noon. This behavior cannot be explained by a spectral mismatch of the filter radiometer or by the missing $j(O^1D)$ temperature dependence. Interestingly, the deviations show some resemblance with the diurnal profiles of the ambient temperature. This is, however, difficult to understand, because both filter radiometers were temperature stabilized. Another possible explanation for the asymmetries would be strong azimuthal anisotropies of the entrance optic sensitivities.

3.4. Irradiance- Versus Actinic-Flux-Based $j(O^1D)$ Values

[51] During the IPMMI campaign the NIWA spectroradiometer measured spectral UV irradiances, which were used instead of actinic fluxes to calculate pseudo $j(O^1D)$ values. The comparison of this data with the measurements by SR-FZJ and SR-NCAR has been presented in detail by *McKenzie et al.* [2002] and will not be repeated here. The authors report $j(O^1D)$ ratios for FZJ/NIWA and NCAR/NIWA that vary from 1.25 at local noon to an approximate value of 3 at sunrise and sunset. This kind of variability is to be expected since the cosine weighting inlet optic of an irradiance spectroradiometer receives less radiation than actinic flux sensors. *McKenzie et al.* [2002] find that the calibration of the NIWA spectroradiometer is in good quantitative agreement (~10%) with the calibrations of the FZJ and NCAR spectroradiometers, when the fundamental differences in the viewing geometries are considered. This agreement is consistent with the specified calibration errors.

4. Molecular Data Recommendations for the Determination of $j(O^1D)$

4.1. Sensitivity of $j(O^1D)$ to the Choice of σ and Φ Data

[52] In order to derive values of $j(O^1D)$ from actinic flux measurements, ozone molecular parameter data must be used. An overview of the available laboratory ozone cross sections and quantum yields and the general uncertainties are given by *Cantrell et al.* [2003]. In general, there appears to be very good agreement in the reported absorption cross sections of ozone [e.g., *Bass and Paur*, 1985; *Molina and Molina*, 1986; *Malicet et al.*, 1995]. This is reflected in the $j(O^1D)$ values which have been calculated for the different cross sections using the same quantum yield [*Talukdar et al.*, 1998] in each case. In Figure 5 (top) the j values are plotted as ratios to the data derived for the cross sections by *Molina and Molina* [1986] and show overall agreement within about 1–3% under the conditions of IPMMI.

[53] In case of the $O(^1D)$ quantum yield the situation is more complicated. Several groups [e.g., *Brock and Watson*, 1980; *Trolier and Wiesenfeld*, 1988; *Ball et al.*, 1993, 1997; *Michelsen et al.*, 1994; *Takahashi et al.*, 1996, 1998; *Talukdar et al.*, 1997, 1998; *Bauer et al.*, 2000; *Smith et al.*, 2000] have reported significant, i.e., nonzero, quantum yields for $O(^1D)$ formation at progressively longer wavelengths, in contrast to the general recommendations that were valid until 1997 [e.g., *DeMore et al.*, 1994]. The more recent laboratory studies agree well and give clear evidence that at wavelengths greater than the threshold of 310 nm, there is significant formation of $O(^1D)$ owing to two processes. One is the photodissociation of vibrationally excited ozone molecules

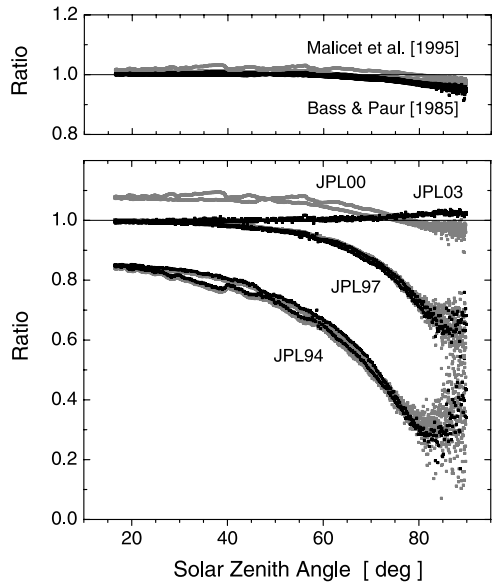

Figure 5. Ratio of $j(O^1D)$ calculated for different ozone molecular parameter data relative to the case with σ by *Molina and Molina* [1986] and Φ by *Talukdar et al.* [1998]. (top) Sensitivity to different published cross section data, using in each case the same quantum yield. (bottom) Sensitivity to different NASA-JPL recommendations for the $O(^1D)$ quantum yield, using in each case the same ozone absorption cross sections. The *j* values have been determined from solar actinic flux spectra measured on 19 June (upper panel: SR-NCAR; lower panel: SR-NCAR in grey; SR-FZJ in black).

up to a cut-off near 325 nm, the other is the spin-forbidden dissociation beyond 325 nm (see review by *Matsumi et al.* [2002]). Recent work by *Bauer et al.* [2000] suggests that the threshold for production of $O(^1D)$ may even extend to 375 nm or beyond. In consequence, derived values of $j(O^1D)$ can be significantly higher than previously thought. Although the ozone absorption cross section decreases rapidly at $\lambda > 320$ nm, a small quantum yield at long wavelengths can contribute significantly to the overall photolysis frequency as a result of the increasing spectral actinic flux, particularly at high solar zenith angles (Figure 1).

[54] The progress in understanding the $O(^1D)$ formation in O_3 photolysis is reflected in several revisions of the quantum yield recommendation published by National Aeronautics and Space Administration (NASA)-Jet Propulsion Laboratory (JPL). The effect of the changes on the derived *j* values is considerable as can be seen in Figure 5. The lower panel shows the ratios of $j(O^1D)$ for the different quantum yields relative to $j(O^1D)$ determined for the data by *Talukdar et al.* [1998], using the same O_3 cross section [*Molina and Molina*, 1986] in each case. Clearly, the revisions since 1994 have led to significantly higher *j* values, in particular at high solar zenith angles. The JPL97 data [*DeMore et al.*, 1994] differ from the JPL94 data [*DeMore et al.*, 1997] by including the contribution from the photolysis of vibrationally excited O_3. The JPL00 [*Sander et al.*, 2000] and JPL03 data [*Sander et al.*, 2003] furthermore contain the contribution of spin-forbidden $O(^1D)$ formation in the O_3 photolysis. The JPL03 data are identical with the current International Union of Pure and Applied Chemistry (IUPAC) recommendation (http://www.iupac-kinetic.ch.cam.ac.uk; data sheet POx2 from 2001) as both have adopted their data from the recommendation by *Matsumi et al.* [2002].

4.2. Comparison of $j(O^1D)$ Derived From Actinic Flux Measurements to Absolute Chemical Actinometer Measurements

[55] One of the aims of IPMMI was to ascertain which of the recently revised molecular data provide the most accurate description of $O(^1D)$ formation in the photolysis of tropospheric ozone for the conditions of IPMMI. Within experimental uncertainty it is clear that the derived values of $j(O^1D)$ are not very sensitive to the choice of literature ozone absorption cross sections. It is also clear from the previous analysis that the derived value of $j(O^1D)$ is quite sensitive to the choice of the $O(^1D)$ quantum yield. The comparison of an absolute technique for the determination of $j(O^1D)$ such as chemical actinometry against actinic flux derived measurements of the photolysis frequency has the potential, within experimental uncertainty, to aid in the choice of molecular parameters. The actinic flux data measured by the NCAR spectroradiometer have been combined with the quantum yield data of *Talukdar et al.* [1998], JPL94, JPL97, and JPL00. In all cases, the cross sections of *Molina and Molina* [1986] were used and temperature was applied as measured inside the chemical actinometer.

[56] The data in Figure 6 show the change in the ratio of $j(O^1D)$ of the chemical actinometer to the NCAR spectroradiometer versus the slant atmospheric ozone column for the four chosen quantum yield data. The slant ozone column has been calculated as the product of measured total ozone (compare Table 4) and the air mass factor estimated as the reciprocal cosine of the solar zenith angle. Here, the slant ozone column serves as a qualitative measure for the red shift of the spectral distribution of $j(O^1D)$ as the absorption of solar ultraviolet radiation increases with total ozone or increasing path length through the atmosphere [cf. *Müller et al.*, 1995; *Shetter et al.*, 1996]. Note that the slant ozone columns in Figure 6 correspond to solar zenith angles from about 16° to approximately 78°.

[57] Figure 6 shows that in general, the ratio of spectroradiometer to chemical actinometer $j(O^1D)$ data is consistent for all four days with and without clouds. In order to reduce the noise, the data points from all days were averaged in bins of slant ozone columns (100 DU width). The corresponding mean values and their standard deviations are displayed as open circles with 1σ error bars. It can be noted that on the days 18 and 19 June (green and red symbols, respectively) the plotted data points separate into two diverging branches at slant ozone columns above 1100 DU. The up- and downward bending branches correspond to measurements at sunrise and sunset, respectively, and are due to a baseline drift of the actinometer readings. This problem is related to the rather indirect determination of $O(^1D)$ in the actinometer. The NCAR instrument uses the reaction of $O(^1D)$ radicals with N_2O to produce NO molecules which are finally oxidized to N_2O_5 (see section 2.1.1). The N_2O_5 then reacts with water on the surface of a semi-permeable membrane to form NO_3^- ions which are detected by a total conductivity measurement. The total conductivity includes any residual

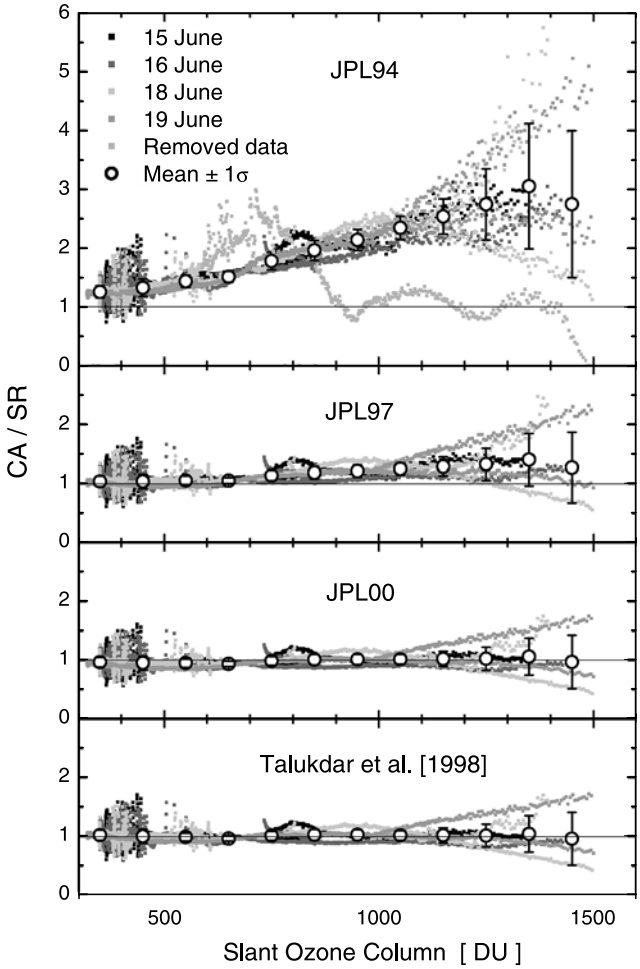

Figure 6. Ratio of $j(O^1D)$ measured by the chemical actinometer and the NCAR spectroradiometer versus the slant ozone column for the days 15–19 June. The spectroradiometer data were evaluated for σ by *Molina and Molina* [1986], different quantum yields (JPL94, JPL97, JPL00, and *Talukdar et al.* [1998]), and the temperature of the actinometer. The open circles represent binned averages over all days for bin widths of 100 DU. The grey symbols in the upper panel have been excluded from the averaging (see text) and are not shown in the other panels. See color version of this figure at back of this issue.

conductivity of the deionized water, conductivity added to the water flow from ozone/wall or ozone/impurities reactions. In this case the determination of $O(^1D)$ depends on the measurement of a small signal difference superimposed on a large conductivity background signal. Baseline drifts can thus produce significant systematic errors in the $j(O^1D)$ measurements when the photolytic $O(^1D)$ production is low as during sunrise and sunset.

[58] In the upper panel of Figure 6 some data points (marked as grey symbols) show large irregular systematic deviations from the bulk of the other data that exhibit a relative coherent trend versus the slant ozone column. The grey marked data were measured on 16 June after 1817 MDT (slant ozone column >850 DU) and on 18 June at 0756–0841 MDT (589–788 DU). In these instances no unusual meteorological conditions were observed that affect $j(O^1D)$ and could explain a different response of the chemical actinometer and spectroradiometer. The irregular deviations are more likely caused by an instrumental measurement problem. When the actinometer signals are compared with the measurements of any of the other radiometers, essentially the same deviation pattern is observed. Thus the unusual behavior must be due to the chemical actinometer and was presumably caused by an unstable baseline as outlined before. For this reason, the grey marked data are treated as outliers. Accordingly, they were excluded from the averaging and are not shown in the other panels.

[59] In the upper panel (case JPL94) an increasing trend is seen for the averaged $j(O^1D)$ ratio as the slant ozone column increases, starting from a ratio of 1.25 at 350 DU and exceeding a factor 2.5 beyond 1100 DU. This observation points to an increasing underestimation of the $O(^1D)$ production in the JPL94 quantum yield at long wavelengths and agrees with previous observations by *Müller et al.* [1995] and *Shetter et al.* [1996]. In case of JPL97 the situation is much improved. The trend is smaller and goes from a mean ratio of 1.04 at 350 DU to as much as a factor 1.4 at 1350 DU, indicative of missing $O(^1D)$ production from the quantum yield data.

[60] In case of JPL00 and *Talukdar et al.* [1998] there is excellent agreement between the chemical actinometer measurements and the actinic flux derived j values. The mean $j(O^1D)$ ratios deviate no more than 5% from unity over the whole range of slant ozone columns, which is much better than what can be expected from the experimental uncertainty of the chemical actinometer (11%) and the actinic flux calibration of the spectroradiometer (6.6%). Strictly, no preference can be given to either of the two quantum yield data within experimental uncertainties. Nevertheless, it appears that JPL00 binned ratios show a slight trend with the total ozone column (0.95 at 300–700 DU, 1.00 at 700–1100 DU, 1.02 at 1100–1500 DU) which is not present in the case of the Talukdar et al. data (1.00 at 300–700 DU, 1.02 at 700–1100 DU, 1.01 at 1100–1500 DU). At small ozone columns the JPL00 binned ratios are a bit smaller than in the Talukdar et al. case, which can be explained by the different short wavelength quantum yields (0.95 versus 0.89). The fact that the use of the quantum yields by *Talukdar et al.* [1998] produces no trend in the $j(O^1D)$ ratio versus slant ozone column is an important criterion in favor of their data. It suggests that the relative wavelength- and temperature-dependence of the quantum yields is sufficiently correct to reproduce the variations of the chemical $j(O^1D)$ measurements encountered under the conditions during IPMMI. Noting that the data for *Talukdar et al.* [1998] agree very well with the JPL03 case (compare Figure 5), this analysis gives support that the most recently recommended $O(^1D)$ quantum yield data are indeed most suitable to determine tropospheric $j(O^1D)$ from measured actinic flux spectra.

5. Comparison of Modeled and Measured Data

[61] As part of IPMMI twelve different groups (Table 2) contributed fifteen model simulations of $j(O^1D)$ for the clear day (19 June) by running various radiative transfer

Table 6. Models and Input Parameters Used for the Calculation of Actinic Flux and Derived $j(O^1D)$ Data[a]

		Cross Section[b]		Quantum Yield[b]	Temperature[c]	
Group	Model Name	Actinic Flux	*j* Value	*j* Value	Actinic Flux	*j* Value
ACD	TUV 4.0	MM	MM	JPL97	sonde	ambient
AES	JMAM	MM	WMO	JPL97	US 1976	297.8 K
BAS	BASRTM	MAL	JPL97	JPL97	US 1976	ambient
BM1	LibRadtran	MM	MM	TAL	US 1976	ambient
BM2	LibRadtran	MM	MM	TAL	US 1976	ambient
BM3	LibRadtran	MM	MM	TAL	US 1976	ambient
JHU	JHU/APL	MM	MM	JPL97	US 1976	ambient
KFA	ART	WMO	MAL	MIC	sonde	ambient
KFU	TUV 3.9	WMO	MM	JPL97	sonde	288.3 K
KNM	DAK	BP	BP	SHE	sonde	288.15 K
MAR	Parametric	MM	MM	SHE	–	–
NIL	LibRadtran	BP	BP	TAL	sonde	ambient
NI2	Phodis	MM	MM	JPL97	sonde	297.8 K
NOA	TUV 3.8	MM	MM	JPL97	US 1976	ambient
UMU	STAR	BUR	BUR	STO	US 1976	ambient

[a]Further model information can be found in the paper by *Bais et al.* [2003].
[b]BP, *Bass and Paur* [1985]; BUR, *Burrows et al.* [1999]; JPL97, *DeMore et al.* [1997]; MAL, *Malicet et al.* [1995]; MIC, *Michelsen et al.* [1994]; MM, *Molina and Molina* [1986]; SHE, *Shetter et al.* [1996]; STO, *Stockwell et al.* [1990]; TAL, *Talukdar et al.* [1998]; and WMO, *WMO Global Ozone Research and Monitoring Project* [1985].
[c]Ambient, see Figure 2a, lowest panel; sonde, daily ozonesonde measurement (19 June: 297.75 K at ground level); US 1976, temperature of the U.S. Standard Atmosphere (1976) (276.9 K at the altitude of the site).

equation solvers. Input data were handled in different ways and different cross sections, quantum yields, and temperatures were used for the calculation of $j(O^1D)$ (Table 6). The various models (except NI2) and treatment of input data have been described and discussed in detail by *Bais et al.* [2003]. The NI2 model has been described elsewhere by *Kylling et al.* [1995]. The version used here is based on the pseudospherical version of the DISORT algorithm [*Stamnes et al.*, 1988; *Dahlback and Stamnes*, 1991].

[62] *Bais et al.* [2003] compared the actinic flux spectra obtained by these models with model reference spectra and measured spectra. In this paper, the modeled $j(O^1D)$ results are compared with $j(O^1D)$ data derived from the measured actinic flux spectra from the FZJ spectroradiometer. It should be noted that this is a blind intercomparison. The modelers did not have access to the measured results prior to submitting their results. However, some groups resubmitted results after obvious misinterpretations of what data was to be submitted or to correct errors that had been discovered after first data submission (for more information, see *Bais et al.* [2003]).

[63] Figure 7 shows ratios of the 10-min data of modeled to experimental $j(O^1D)$ values. In this comparison the experimental spectroradiometer data make use of the same or similar molecular parameters and temperatures as were used by the models. This procedure allows to investigate how well the models simulate the ultraviolet part of solar radiation that drives $O(^1D)$ formation in the troposphere. The different quantum yields, cross sections and temperatures used by the models are given in Table 6. The spectroradiometer evaluation uses absorption cross sections by *Molina and Molina* [1986] and ambient temperatures. Those models using quantum yields by *Shetter et al.* [1996], JPL97 [*DeMore et al.*, 1997], *Michelsen et al.* [1994], and *Stockwell et al.* [1990] are compared with spectroradiometer results using the JPL97 quantum yields. The models using data by *Talukdar et al.* [1998] are compared with FZJ spectroradiometer data using the same quantum yield.

[64] Discrepancies between the various models and the experimental results may be due to one or more of several reasons.

5.1. Uncertainties in the Radiative Transfer Equation (RTE) Solver

[65] Various methods to solve the equation of radiative transfer were used by different participants. Many of the methods may be called exact in the sense that they are capable of solving the plane-parallel RTE exactly for the given input conditions. In other words, the uncertainty of the model result is only determined by the uncertainty of the input parameters, including absorption cross sections, quantum yields and the extraterrestrial flux. This is the case, for example, for the Discrete Ordinate method, the Monte Carlo method and the Matrix Operator method. None of the models, however, used a fully spherical solver, for which reason the differences increase with increasing solar zenith angle. In some cases (BM1, BM3, KNM, MAR) no correction for spherical geometry was used, while in most cases the so-called pseudo-spherical approximation was employed. The BM2 and BM3 models are identical except that BM3 used plane-parallel and BM2 pseudospherical geometry. The ratio of BM3 over BM2 has a value of approximately one for solar zenith angles up to 65°. At larger zenith angles the plane-parallel approximation increasingly underestimates the $j(O^1D)$ values, for example, by 10% at SZA = 80° and ~80% at SZA = 90°.

5.2. Differences in the Extraterrestrial Flux

[66] The different extraterrestrial fluxes used by the modelers cause differences of up to 7%. The majority of modelers have used the ATLAS-3 extraterrestrial spectrum, which is one of the most recent and most widely accepted. Among the solar spectra used by the other models, MODTRAN 3 (used by the JHU model) produces the largest difference (approximately +7%) in $j(O^1D)$ relative to ATLAS-3. *Bais et al.* [2003] discusses the spectral differences between the extraterrestrial spectra in some detail. A discussion of various extraterrestrial spectra is provided by *Woods et al.* [1996].

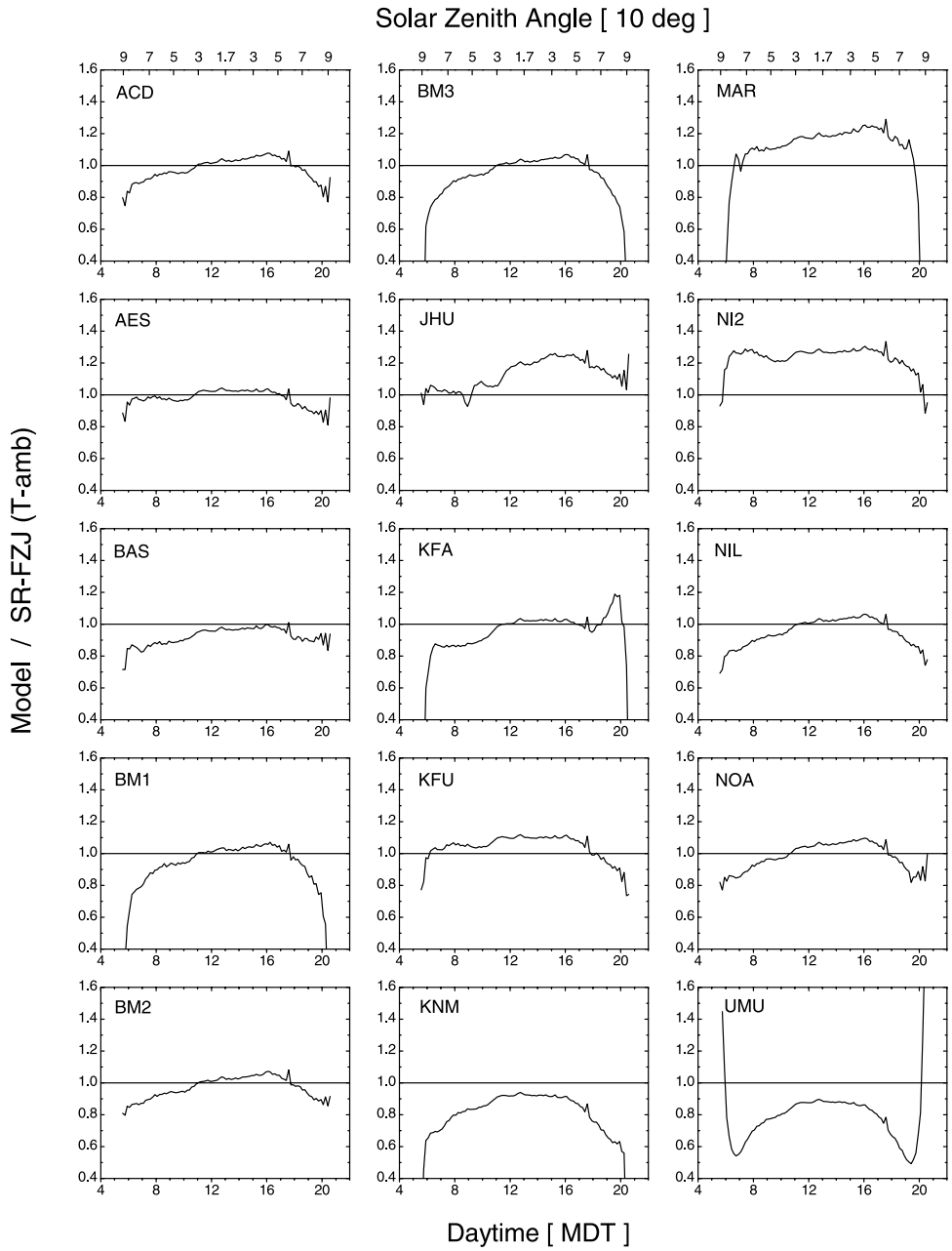

Figure 7. Ratios of 10-min data of $j(O^1D)$ calculated with the various models and as derived from the FZJ spectroradiometer measurements. The models use cross sections, quantum yields, and temperatures that are listed in Table 6. The spectroradiometer data are evaluated using ozone cross sections by *Molina and Molina* [1986] and ambient temperatures. Models that use quantum yields from JPL97, *Shetter et al.* [1996], *Michelsen et al.* [1994] and *Stockwell et al.* [1990] are compared with spectroradiometer data using JPL97. Models using quantum yields by *Talukdar et al.* [1998] are compared with spectroradiometer data using the same quantum yield. Note that the ordinate scale begins at 0.4.

[67] Extraterrestrial solar spectra are usually published for vacuum wavelengths. For the calculation of $j(O^1D)$ in air at the Earth's surface, the wavelength scale must be shifted by $\sim$0.1 nm toward shorter wavelengths. The model ACD did not apply this correction which leads to an overestimation of $j(O^1D)$ by about 2–3%. Another source of systematic error related to the extraterrestrial solar flux is the Earth-Sun distance, which varies throughout the year because of the eccentricity of the Earth's orbit. The extraterrestrial fluxes are usually specified for Earth-Sun distance of 1 AU (Astronomical Unit) which occurs at the equinoxes. During the IPMMI campaign the Earth was further away from the Sun, reducing the radiation by 3% compared with equinox. All model results except for AES were corrected for the Earth-Sun distance.

5.3. Differences in Atmospheric Parameters

[68] The vertical profiles of air pressure, temperature, ozone concentration, aerosol number density and aerosol optical properties are important input parameters for the

modeling of $j(O^1D)$. At high Sun, $j(O^1D)$ at the surface is mainly determined by the vertically integrated columns of air, ozone and aerosols, and only to a smaller degree by their vertical distributions. With increasing solar zenith angle, however, the influence of the profiles becomes more important, for which reason differences in the profiles can lead to significant differences in the photolysis frequencies at ground.

[69] In the IPMMI case, vertical profiles of pressure, temperature, and ozone were provided as measured sonde data up to a height of 35 km. In addition, measurements of vertically integrated columns of air, ozone, and aerosol optical depth (AOD) were made available. Aerosol optical properties were available only as measurements at 5 m above ground. Details about handling these model input parameters are given by *Bais et al.* [2003]. It should be noted that on the basis of preliminary ozone data, a total ozone column value of 300 DU was given to the modelers for the day of 19 June, whereas the actual value was 306 DU. Because of this systematic error all modeled $j(O^1D)$ values are increased by about 3–4% at SZA $< 75°$.

[70] Despite the relatively low AOD value (0.03 ± 0.02) on the day of 19 June, the use of different aerosol profiles and aerosol optical properties has a significant influence on the calculated $j(O^1D)$ values. An example is the NI2 model which did not include aerosols, leading to an overestimation of $j(O^1D)$ by about 5% at noon. While most models used the prescribed time-independent values of AOD and aerosol optical properties, JHU model calculations used aerosol optical-depth values which were scaled to the variable AOD at 1020 nm measured during IPMMI. This different data handling explains the different diurnal variability of the JHU results [*Swartz*, 2002].

5.4. Differences in Molecular Parameters

[71] Six different ozone absorption spectra were in use by the various participants (see Table 6). The ozone cross section is used both to calculate the actinic flux and to calculate the $j(O^1D)$ photolysis frequency. Most participants (except AES, BAS, KFA, and KFU) used the same cross section for both calculations. The ozone cross section is temperature dependent. This dependence was accounted for using either the US standard atmosphere or the ozone sonde measurements (Table 6). It is noted that KNM used cross-section data by *Bass and Paur* [1985] at vacuum wavelengths for the actinic flux calculations with temperature dependence included, and used air wavelengths at a fixed temperature of 288.15 K for the $j(O^1D)$ rate. The effect of using different ozone cross sections was investigated by running one of the models, NIL, with either the *Molina and Molina* [1986] or the *Bass and Paur* [1985] cross sections and keeping everything else constant. The results indicate that the use of different cross sections at most caused a difference of 3% in $j(O^1D)$ at solar zenith angles less than 75°.

[72] Quantum yields from five sources were used by the various models. The differences in $j(O^1D)$ expected from the use of the different quantum yields are shown in Figure 5. Note that the use of the quantum yields by *Michelsen et al.* [1994] and *Shetter et al.* [1996] produce similar results compared to the use of JPL97 data, while the quantum yields by *Stockwell et al.* [1990] are similar to the JPL94 case. It should be noted that the differences in Figure 5 do not show up in Figure 7, as the model results are compared to experimental data derived for similar quantum yields.

[73] The quantum yield depends on temperature. This dependence was accounted for using the ambient temperature measurements which varied between 287.19–306.55 K and had a value of 299.3 K at noon. Two groups (AES and NI2) calculated $j(O^1D)$ for a fixed temperature of 297.8 K which is an appropriate value for the noontime of 19 June, but leads to an over- or underestimation of $j(O^1D)$ by up to 10% in the morning and afternoon, respectively. In case of KFU and KNM even larger deviations result from using a fixed temperature of 288.3 K. The relatively low temperature fits the conditions at sunrise of 19 June, but results in $j(O^1D)$ values which are too low by 10–20% in the afternoon.

5.5. General Discussion

[74] Eight of the models (ACD, AES, BAS, BM2, KFA, KFU, NIL, NOA) agree with the measurements within 15% for solar zenith angles smaller than 75°. Two of these models (AES, KFU) have used a fixed temperature for the calculation of the photolysis frequencies. If corrected for this effect, the AES model results would be slightly lower in the morning and slightly higher in the afternoon by as much as 10%. In case of KFU the corrected $j(O^1D)$ values would be generally higher during the day, reaching about +20% in the afternoon.

[75] Two other models (MAR, NI2) show relatively high ratios, which can be explained partly (~5%) by the aerosols missing in the two models. The JHU ratio is relatively high between 10:00 and 18:00 MST and shows a diurnal structure which is not found in the results of other models. This behavior can be explained by the use of different model input parameters for the extraterrestrial spectrum and for aerosol. Recalculations by JHU, using the ATLAS-3 extraterrestrial spectrum instead of Modtran-3 and the prescribed IPMMI aerosol specifications, show similar good agreement with the measurements like other models, e.g., ACD [*Swartz*, 2002].

[76] For larger solar zenith angles the differences generally increase with the model values being smaller than the measured values. In case of the BM1, BM3, KNM, and MAR models this may be partly explained by the plane-parallel assumption applied in the radiative transfer equation solvers as discussed before. More generally, part of the deviations at high solar zenith angles can be explained by the prescribed ozone column, which was 2% higher than the actual value, and in some cases by the use of the *Molina and Molina* [1986] cross sections, while the ozone column was derived using the absorption data by *Bass and Paur* [1985]. *Bais et al.* [2003] discuss this issue in some detail with respect to the actinic flux. They show that the spectral deviations become larger at shorter wavelengths below 320 nm and increase furthermore with solar zenith angle.

[77] The models KNM and UMU deviate from the $j(O^1D)$ measurements with a relatively strong solar zenith dependence, whereas the corresponding comparison of modeled and measured actinic flux spectra shows good

agreement [*Bais et al.*, 2003]. Besides the plane-parallel assumption applied in the KNM model, the trends are most likely related to the $O(^1D)$ quantum yield and its temperature dependence. KNM used a similar quantum-yield [*Shetter et al.*, 1996], but used a temperature that is too low, while the deviations of the UMU model are likely explained by the choice of outdated quantum yields [*Stockwell et al.*, 1990], which are similar to the JPL94 case.

6. Conclusions

[78] Different measurement techniques for $j(O^1D)$ were blindly compared to each other in the framework of IPMMI. The comparison was made for the downwelling 2π sr component of $j(O^1D)$ at the ground over four days at high- to low-Sun conditions (SZA = 16.5°–90°). Moreover, theoretical $j(O^1D)$ model results were blindly compared to the data measured on one day with clear sky and relatively low aerosol optical density.

[79] Eleven instruments, operated by six groups, participated in the experimental comparison for $j(O^1D)$. The instruments included one chemical actinometer, six spectroradiometers, and four filter radiometers. General good agreement with deviations less than 10% among all radiometers (SR, FR) was found for solar zenith angles less than 60°, provided that the instruments used similar absorption cross sections, quantum yields, and temperatures for deriving the $j(O^1D)$ values. This result is consistent with the specified errors given for the instrumental calibrations. Deviations up to 14% were observed when $j(O^1D)$ was derived for a fixed temperature (25°) rather than for the actual temperature variations. In one case, temporary condensation of humidity in the inlet optic caused slightly elevated radiometer signals up to 12%.

[80] At solar zenith angles between 60° and 85° some radiometers showed deviations which were as high as a factor of 2. Possible reasons are nonlinearities of the radiation detectors or anisotropic behavior of the radiation collector optics. In case of one spectroradiometer, which used a single-monochromator rather than a double-monochromator, internal stray-light was found to be a problem. Insufficient correction for the monochromator stray-light signal caused disagreements that significantly increased at solar zenith angles greater than 60°. In the same range of zenith angles some of the filter radiometers showed significant deviations because of insufficient correction for the imperfect match of the spectral radiometer response to the photodissociation spectrum of $O_3 \rightarrow O(^1D)$.

[81] Three of the radiometers (SR-NCAR, SR-FZJ, and FR-FZJ*) showed excellent agreement with each other and with the chemical actinometer at all solar zenith angles up to at least 80° within typically 5%. These radiometers used the $O(^1D)$ quantum yield data by *Talukdar et al.* [1998] and explicitly considered the temperature dependence of $j(O^1D)$. This good agreement demonstrates that each of the different categories of instruments (CA, SR, FR) is capable of accurate determinations of $j(O^1D)$.

[82] The comparison of one reference radiometer (SR-NCAR) with the chemical actinometer was used to investigate the sensitivity of derived $j(O^1D)$ values to the choice of published data for σ and ϕ. It was also used to determine which of the different $O(^1D)$ quantum yield recommendations (JPL-94, JPL-97, JPL-00, JPL03) provides the best description for $j(O^1D)$ in the troposphere. Within experimental uncertainty the derived values of $j(O^1D)$ are not very sensitive to the choice of literature ozone absorption cross sections. A large sensitivity, however, was found to the choice of data for the $O(^1D)$ quantum yield. The significant improvement in understanding the ozone photodissociation processes obtained in recent laboratory studies [*Matsumi et al.*, 2002] is confirmed by the excellent agreement between $j(O^1D)$ values measured by the chemical actinometer and the spectroradiometer using recently published quantum yields. At SZA < 80° the mean deviations are smaller than 5% which is less than what is expected from the instrumental uncertainty (11%) of the chemical actinometer. The IPMMI study thus gives support to the most recent quantum yield recommendation by JPL03 [*Sander et al.*, 2003] and IUPAC (http://www.iupac-kinetic.ch.cam.ac.uk; data sheet POx2 from 2001).

[83] It should be noted that the good agreement in the IPMMI comparison between chemical actinometry and actinic flux spectroradiometry implicitly includes the effect of temperature on $j(O^1D)$ between 5°C and 45°C. This does not cover the range of temperatures encountered in the free troposphere, for which a further intercomparison would be desirable. The estimated effect of temperature at ground is on the order of 1% K^{-1} and depends on the solar zenith angle and vertically integrated ozone column as is discussed by *Bohn et al.* [2004].

[84] Twelve model groups participated in the comparison of theoretically modeled $j(O^1D)$ with measured data. Fifteen different models were operated that included relatively simple parametric methods to more sophisticated radiative transfer solvers like the DISORT method. For the chosen conditions (clear sky with relatively low aerosol optical density) most models agreed within 15% with the spectroradiometer derived $j(O^1D)$ values at SZA < 75°, provided that they used similar absorption cross sections, quantum yields, and temperatures as the experimental method. Deviations can be attributed to uncertainties in the radiative transfer solvers (e.g., plane-parallel atmosphere assumption), differences in the extraterrestrial solar fluxes, treatment of atmospheric parameters (e.g., vertical profiles of ozone, aerosols etc.) and molecular parameters. As in the case of spectroradiometry, the proper choice of the $O(^1D)$ quantum yields and temperature was found to be very important to obtain accurate photolysis frequencies. Note that IPMMI has not performed a model to measurement comparison for cloudy conditions. This needs to be done in future work that addresses the complex influence of clouds on the solar actinic flux.

Appendix A: Instrumental Descriptions

A1. Descriptions of the Spectroradiometers

A1.1. SR-FZJ

[85] The scanning actinic flux spectroradiometer of Forschungszentrum Jülich has been described in detail by *Hofzumahaus et al.* [1999]. During IPMMI, the instrument consisted of a 2π sr entrance optic (METCON/FZJ), a scanning double monochromator (Bentham DTM 300), a

10 m quartz fiber-optic bundle (Gigahertz Optik GmbH), a photoelectric detection system (EMI 9250 photomultiplier), and a computer for data acquisition and system control. Spectra from 280 nm to 420 nm were typically scanned every 80 s (68 s to scan the spectra), with a step size of 1.0 nm and a spectral band pass (full width at half maximum (FWHM)) of 1.1 nm. Absolute spectral calibrations were performed with a PTB-traceable irradiance standard (FEL 1000 W quartz lamp, Gigahertz Optik GmbH) on the field site on the days 14, 17, and 20 June. Additional field calibrations were performed with secondary standards (200 W and 45 W quartz lamps) to monitor the relative stability of the instrumental sensitivity on each day of the campaign. Wavelength calibrations of the monochromator were performed using emission lines of a mercury lamp and by examination of the Fraunhofer structure in the solar spectrum.

A1.2. SR-MET1 and SR-MET2

[86] Meteorologie Consult GmbH, Glashütten (METCON) deployed two commercially available spectroradiometers for IPMMI. The double-monochromator spectrometer instrument (SR-MET1) consisted of a 2π sr entrance optic (METCON), a double monochromator (CVI-Digikrom CM 112), a photomultiplier tube (Hamamatsu R759), and a computer for data acquisition. Spectra from 280 nm to 420 nm with 1 nm increments were scanned in under 90 s with a spectral band pass (FWHM) of 1 nm. Calibrations of the absolute and relative spectral sensitivity were performed prior to the intercomparison using the 1000 W NIST-traceable irradiance-standard lamp in the NCAR laboratory calibration facility. Wavelength calibrations for the SR-MET1 instrument were performed once per day with a mercury lamp. In addition, high-resolution (0.1 nm) scans of the Fraunhofer lines were performed every 100 data scans.

[87] The photodiode-array spectrometer instrument (SR-MET2) consisted of a 2π sr entrance optic (METCON), ceramic single monochromator (METCON/Carl Zeiss), a photodiode-array detector (Hamamatsu S3904-512Q), and a computer for data acquisition. Spectra from 280 nm to 650 nm were measured in under 5 s for $j(O^1D)$ with a spectral band pass (FWHM) of 2.1 nm and a pixel resolution of 0.83 nm. For the photodiode-array spectrometer, only relative spectral calibrations were performed versus the 1000 W NCAR lamp. Accordingly, field data were evaluated as relative j values in arbitrary units, which were then scaled to the calibrated data of the SR-MET1 instrument. Wavelength calibrations were performed once before the experiment and then by a permanent crosscheck with Fraunhofer lines in the solar spectrum during conversion from raw data to j data.

A1.3. SR-NCAR

[88] The NCAR scanning actinic flux spectroradiometer has been described in detail by *Shetter and Müller* [1999]. As installed during IPMMI, the instrument consisted of a 2π sr entrance optic (METCON/NCAR), a 12 m custom fiber-optic bundle with high UV throughput (CeramOptec), a double monochromator (CVI Digikrom CM 112), photomultiplier tube (Electron Tubes, Ltd.), a custom-designed four-stage current-to-voltage amplifier, and a computer for fully automated data acquisition and system control. Spectra from 280 nm to 420 nm were scanned every 15 s (11 s to scan the spectra) by stepping in 1.0 nm increments in the range of 280–330 nm and 2.0 nm increments in the range of 330–420 nm. The spectral band pass (FWHM) was 1.0 nm. Absolute spectral calibrations were performed with a NIST-traceable irradiance standard (1000 W quartz-tungsten-halogen (QTH) lamp, Oriel Instruments, 63350) in the NCAR laboratory before and after the intercomparison. Field calibrations were performed with secondary lamps (250 W, QTH) for several weeks before, during (17 June), and after the project to assess the relative stability of the instrument sensitivity. Wavelength calibrations of the monochromator were performed in conjunction with each spectral calibration using the emission lines from a mercury lamp.

A1.4. SR-ULI

[89] The University of Leicester deployed a new photodiode-array spectroradiometer that had been manufactured by METCON and is described in detail by *Edwards and Monks* [2003]. The instrument consisted of a 2π sr entrance optic (METCON), a single monochromator (Carl Zeiss), a 512 pixel photodiode-array detection system (Carl Zeiss) and a computer for data acquisition. The photodiode array measured wavelengths from 285 nm to 450 nm in consecutive 0.5, 1, 3 and 5 s integration times with a spectral band pass of 2.2 nm (FWHM) and a pixel resolution of 0.83 nm. An absolute spectral calibration was performed during IPMMI using the 1000 W NIST-traceable irradiance standard in the NCAR laboratory calibration facility. After the intercomparison, the instrument was again calibrated using a 200 W NIST-traceable QTH lamp (Oriel) at the University of Leicester. Wavelength calibrations of the photodiode array were performed using the emission lines from mercury and sodium lamps. During the intercomparison the significant stray-light background of the single monochromator was determined as the average in the range of 285–290 nm and subtracted from the whole spectrum before calculating $j(O^1D)$.

A1.5. SR-NIWA

[90] The irradiance spectroradiometer of the National Institute of Water and Atmospheric Research has been described in detail by *McKenzie et al.* [1992, 2002]. The instrument is based on a Jobin-Yvon double monochromator (JYDH10), configured for a spectral resolution of 1.3 nm. A shaped PTFE diffuser which was designed in-house results in an excellent cosine response. The diffuser is coupled to the spectrometer through a multi-stranded quartz fibre-optic cable. The detector is a photomultiplier (EMI 9804 QA) operated in analogue mode. A diode at the entrance slit monitors intensity changes during the scan. The scan range is 290 nm to 450 nm, with a sampling interval of 0.2 nm and a total scan time of 190 s. During the IPMMI campaign, scans were acquired at 5-min intervals. Irradiance calibration is with reference to NIST scale through 1000 W FEL lamps. Wavelength registration (including corrections for nonlinearities in the wavelength drive) is achieved through correlation alignment against Fraunhofer features as in the LOWTRAN spectrum, degraded to the instrument resolution.

A2. Descriptions of the Filter Radiometers

A2.1. FR-MET

[91] The METCON filter radiometer originates from the concept of *Junkermann et al.* [1989] and includes technical modifications (e.g., different inlet optic design, temperature

stabilization) that improve the measurement stability of the instrument. The entrance optic of the radiometer consists of diffusively transmitting quartz domes and has a nearly uniform angular response to radiation incident from the upper hemisphere (2π sr). The collected radiation is transmitted through an optical interference filter (center wavelength ~300 nm, band pass ~10 nm) and is detected by a solar-blind photomultiplier having a CsTe photocathode. A single-stage current-to-voltage amplifier converts the photocurrent into a voltage signal. Nonlinearities in the relationship between the signal and $j(O^1D)$ are corrected for the SZA and overhead O_3 column using the method described by *Müller* [1994]. The spectral characteristics of the FR-MET filter radiometer as well as the measurements of the overhead O_3 column are used for this correction. The absolute value of the reported $j(O^1D)$ filter radiometer is related to that of the SR-MET1 spectroradiometer.

A2.2. FR-FZJ

[92] The filter radiometer of Forschungszentrum Jülich used during IPMMI was a commercial instrument manufactured by METCON. During IPMMI the filter radiometer signal was recorded by a data logging system with an integration time of 60 s. The filter radiometer was temperature stabilized at (35 ± 1) °C and has been characterized at Forschungszentrum Jülich with respect to its angular and spectral response. The absolute spectral sensitivity was measured in two steps: first the relative response was measured against a tunable radiation source (Xe arc lamp and monochromator, 270–400 nm tuning range, 1 nm bandwidth), using a PTB-calibrated silicon photodiode as a reference. In a second step, the absolute response of the filter radiometer was determined against the irradiance standard (FEL 1000-W quartz lamp, Gigahertz Optik GmbH, PTB-traceable) that was also used for the calibration of the FZJ spectroradiometer during IPMMI. The signal of the filter radiometer is converted into $j(O^1D)$ values applying a nonlinear calibration function that takes into account the angular and spectral characteristics of the radiometer and the temperature-dependent molecular data (σ, ϕ) of reaction (R1) [*Müller*, 1994]. The calibration applied during IPMMI depends on the SZA, overhead O_3 column, and air temperature and is described in detail by *Bohn et al.* [2004].

A2.3. FR-IFU

[93] The filter radiometer of the Institut für Meteorologie und Klimaforschung (former Fraunhofer Institut für Atmosphärische Umweltforschung) uses the METCON inlet system, but the solar-blind photomultiplier of previous designs [*Junkermann et al.*, 1989] has been replaced by a temperature-stabilized combination of a multialkali-UV photodiode (Hamamatsu R448-2), two solar-blind filters (Corion SB-300, center wavelength 300 nm, band pass 85 nm FWHM), and a narrow bandwidth interference filter (Schott UV-MIL, center wavelength 301 nm, band pass 6 nm FWHM). Since the spectral response of the instrument does not match $\sigma\phi$ of reaction (R1) perfectly, a numerical correction is applied to the conversion of the radiometer signals into $j(O^1D)$. The correction algorithm depends on SZA and total O_3 column density and was derived from the comparison of actual instrument spectral sensitivity to the $j(O^1D)$ quantum yield and cross section using a radiative transfer model. Absolute calibration of the IFU filter radiometer was achieved by comparison with a $j(O^1D)$ chemical actinometer at IFU. The actinometer utilizes the chemical reactions (R1), (R5), and (R6) and measures N_2 by gas chromatography, a concept that was first used by *Bahe et al.* [1979].

A2.4. FR-ULI

[94] The $j(O^1D)$ filter radiometer was constructed at University of Leicester and is based on the original concepts by *Junkermann et al.* [1989]. It includes a 2π sr entrance optics that was supplied commercially by METCON. The collected radiation is transmitted via a collimator assembly to an optical interference filter (center wavelength ~300 nm, band pass ~10 nm (FWHM)) and the resultant signal is detected by a solar-blind photomultiplier tube (Hamamatsu, R431S). The photocurrent is converted into a voltage signal via a current-to-voltage amplifier and recorded by a data logging system with an integration time of 60 s. The optical train was temperature stabilized to (30 ± 1) °C. The absolute calibration of the ULI filter radiometer is traceable to a chemical actinometer of Forschungszentrum Jülich [cf. *Müller et al.*, 1995] which uses the same concept as the IFU actinometer. Since the first calibration the absolute and relative spectral sensitivity of the FR-ULI instrument has been controlled for possible drifts against calibrated lamps (200 W, QTH). Drifts were found to be smaller than 1%. For the conditions of IPMMI nonlinearities between the radiometer signal and $j(O^1D)$ have been corrected for the solar zenith angle dependence assuming a constant overhead O_3 column of 350 Dobson Units (DU). Dark current offset was determined daily from radiometer dark current measurements.

[95] **Acknowledgments.** The IPMMI participants are grateful to the National Science Foundation, the National Center for Atmospheric Research, and the WMO Scientific Advisory Group (SA) for UV Monitoring for their financial support of IPMMI. The participation of Forschungszentrum Jülich was supported by the German Federal Ministry for Education, Science and Research (BMBF).

References

Bahe, F., and U. Schurath (1978), Measurement of $O(^1D)$ formation by ozone photolysis in the troposphere, *Pure Appl. Geophys.*, *116*, 537–544.

Bahe, F. C., W. N. Marx, U. Schurath, and E. P. Röth (1979), Determination of the absolute photolysis rate of ozone by sunlight, $O_3 + h\nu \rightarrow O(^1D) + O_2(^1\Delta_g)$, at ground level, *Atmos. Environ.*, *13*, 1515–1522.

Bairai, S. T., and D. H. Stedman (1992), Actinometric measurement of $j\langle O_3\text{-}O(^1D)\rangle$ using a luminol detector, *Geophys. Res. Lett.*, *19*, 2047–2050.

Bais, A. F., et al. (2003), International Photolysis Frequency Measurement and Model Intercomparison (IPMMI): Spectral actinic solar flux measurements and modeling, *J. Geophys. Res.*, *108*(D16), 8543, doi:10.1029/2002JD002891.

Ball, S. M., G. Hancock, I. J. Murphy, and S. P. Rayner (1993), The relative quantum yields of $O_2(a^1\Delta_g)$ from the photolysis of ozone in the wavelength range 270 nm < λ < 329 nm, *Geophys. Res. Lett.*, *20*, 2063–2066.

Ball, S. M., G. Hancock, S. E. Martin, and J. C. Pinot de Moira (1997), A direct measurement of the $O(^1D)$ quantum yields from the photodissociation of ozone between 300 and 328 nm, *Chem. Phys. Lett.*, *264*, 531–538.

Bass, A. M., and R. J. Paur (1985), The ultraviolet cross sections of ozone: I, II, in *Atmospheric Ozone, Proceedings of the Quadrennial Ozone Symposium, Greece*, edited by C. S. Zerefos and A. Ghazi, pp. 606–616, D. Reidel, Norwell, Mass.

Bauer, D. L., D. Ottone, and A. J. Hynes (2000), O^1D quantum yields from O_3 photolysis in the near UV region between 305 and 375 nm, *Phys. Chem. Chem. Phys.*, *2*, 1421–1424.

Blackburn, T. E., S. T. Bairai, and D. H. Stedman (1992), Solar photolysis of ozone to singlet D oxygen atoms, *J. Geophys. Res.*, *97*, 10,109–10,117.

Bohn, B., A. Kraus, M. Müller, and A. Hofzumahaus (2004), Measurement of atmospheric $O_3 \rightarrow O(^1D)$ photolysis frequencies using filter

radiometry, *J. Geophys. Res.*, *109*, doi:10.1029/2003JD004319, in press.

Brauers, T., H.-P. Dorn, H. Koch, A. B. Kraus, and C. Plass-Dülmer (1998), Meteorological aspects, ozone, and solar radiation measurements during POPCORN 1994, *J. Atmos. Chem.*, *31*, 33–52.

Brock, J. C., and R. T. Watson (1980), Laser flash photolysis of ozone: $O(^1D)$ quantum yields in the fall-off region 297–325 nm, *Chem. Phys.*, *46*, 477–484.

Burrows, J. P., A. Richter, A. Dehn, B. Deters, S. Himmelmann, and J. Orphal (1999), Atmospheric remote-sensing reference data from GOME-2: Temperature-dependent absorption cross sections of O_3 in the 231–794 nm range, *J. Quant. Spectrosc. Radiat. Transfer*, *61*, 509–517.

Cantrell, C. A., J. G. Calvert, A. Bais, R. E. Shetter, B. L. Lefer, and G. D. Edwards (2003), Overview and conclusions of the International Photolysis Frequency Measurement and Modeling Intercomparison (IPMMI) study, *J. Geophys. Res.*, *108*(D16), 8542, doi:10.1029/2002JD002962.

Crawford, J., D. Davis, G. Chen, R. Shetter, M. Müller, J. Barrick, and J. Olson (1999), An assessment of cloud effects on photolysis rate coefficients: Comparison of experimental and theoretical values, *J. Geophys. Res.*, *104*, 5725–5734.

Dahlback, A., and K. Stamnes (1991), A new spherical model for computing the radiation-field available for photolysis and heating at twilight, *Planet. Space Sci.*, *39*, 671–683.

DeMore, W. B., S. P. Sander, C. J. Howard, A. R. Ravishankara, D. M. Golden, C. E. Kolb, R. F. Hampson, M. J. Kurylo, and M. J. Molina (1994), Chemical kinetics and photochemical data for use in stratospheric modeling: Evaluation number 11, *JPL Publ., 94-26*.

DeMore, W. B., S. P. Sander, C. J. Howard, A. R. Ravishankara, D. M. Golden, C. E. Kolb, R. F. Hampson, M. J. Kurylo, and M. J. Molina (1997), Chemical kinetics and photochemical data for use in stratospheric modeling: Evaluation number 12, *JPL Publ., 97-4*.

Dickerson, R. R., D. H. Stedman, W. L. Chameides, P. J. Crutzen, and J. Fishman (1979), Actinometric measurements and theoretical calculations of $j(O_3)$, the rate of photolysis of ozone to $O(^1D)$, *Geophys. Res. Lett.*, *6*, 833–836.

Dickerson, R. R., D. H. Stedman, and A. C. Delany (1982), Direct measurements of ozone and nitrogen dioxide photolysis rates in the troposphere, *J. Geophys. Res.*, *87*, 4933–4946.

Eckstein, E., D. Perner, and T. Trautmann (2002), A new actinic flux 4π-spectroradiometer: Instrument design and application to clear sky and broken cloud conditions, *Atmos. Chem. Phys. Discuss.*, *2*, 1939–1977.

Edwards, G. D., and P. S. Monks (2003), Performance of a single monochromator diode array spectroradiometer for the determination of actinic flux and atmospheric photolysis frequencies, *J. Geophys. Res.*, *108*(D16), 8546, doi:10.1029/2002JD002844.

Ehhalt, D. H., H.-P. Dorn, and D. Poppe (1991), The chemistry of the hydroxyl radical in the troposphere, *Proc. R. Soc. Edinburgh, Sect. B: Biol. Sci.*, *97*, 17–34.

Hofzumahaus, A., T. Brauers, U. Platt, and J. Callies (1992), Latitudinal variation of measured O_3 photolysis frequencies $J(O^1D)$ and primary OH production rates over the Atlantic Ocean between 50°N and 30°S, *J. Atmos. Chem.*, *15*, 283–298.

Hofzumahaus, A., A. Kraus, and M. Müller (1999), Solar actinic flux spectroradiometry: A technique for measuring photolysis frequencies in the atmosphere, *Appl. Opt.*, *38*, 4443–4460.

Hofzumahaus, A., A. Kraus, A. Kylling, and C. S. Zerefos (2002), Solar actinic radiation (280–420 nm) in the cloud-free troposphere between ground and 12 km altitude: Measurements and model results, *J. Geophys. Res.*, *107*(D18), 8139, doi:10.1029/2001JD900142.

Junkermann, W. (1994), Measurements of the $J(O^1D)$ actinic flux within and above stratiform clouds and above snow surfaces, *Geophys. Res. Lett.*, *21*, 793–796.

Junkermann, W. (2001), An ultralight aircraft as platform for research in the lower troposphere: System performance and first results from radiation transfer studies in stratiform aerosol layers and broken cloud conditions, *J. Atmos. Oceanic Technol.*, *18*, 934–946.

Junkermann, W., U. Platt, and A. Volz-Thomas (1989), A photoelectric detector for the measurement of photolysis frequencies of ozone and other atmospheric molecules, *J. Atmos. Chem.*, *8*, 203–227.

Kanaya, Y., Y. Kajii, and H. Akimoto (2003), Solar actinic flux and photolysis frequency determinations by radiometers and a radiative transfer model at Rishiri Island: Comparisons, cloud effects, and detection of an aerosol plume from Russian forest fires, *Atmos. Environ.*, *37*, 2463–2475.

Kraus, A., and A. Hofzumahaus (1998), Field measurements of atmospheric photolysis frequencies for O_3, NO_2, HCHO, H_2O_2 and HONO by UV spectroradiometry, *J. Atmos. Chem.*, *31*, 161–180.

Kylling, A., K. Stamnes, and S.-C. Tsay (1995), A reliable and efficient two-stream algorithm for spherical radiative transfer: Documentation of accuracy in realistic layered media, *J. Atmos. Sci.*, *21*, 115–150.

Lefer, B. L., S. R. Hall, L. Cinquini, and R. E. Shetter (2001), Photolysis frequency measurements at the South Pole during ISCAT-98, *Geophys. Res. Lett.*, *28*, 3637–3640.

Levy, H., II (1972), Photochemistry of the lower troposphere, *Planet. Space Sci.*, *20*, 919–935.

Levy, H., II (1974), Photochemistry of the troposphere, *Adv. Photochem.*, *9*, 369–523.

Madronich, S. (1987), Photodissociation in the atmosphere: 1. Actinic flux and the effects of ground reflection and clouds, *J. Geophys. Res.*, *92*, 9740–9752.

Malicet, J., D. Daumont, J. Charbonnier, C. Parisse, A. Chakir, and J. Brion (1995), Ozone UV spectroscopy. II. Absorption cross-sections and temperature dependence, *J. Atmos. Chem.*, *21*, 263–273.

Matsumi, Y., F. J. Comes, G. Hancock, A. Hofzumahaus, A. J. Hynes, M. Kawasaki, and A. R. Ravishankara (2002), Quantum yields for production of $O(^1D)$ in the ultraviolet photolysis of ozone: Recommendation based on evaluation of laboratory data, *J. Geophys. Res.*, *107*(D3), 4024, doi:10.1029/2001JD000510.

McElroy, C. T., C. Midwinter, D. V. Barton, and R. B. Hall (1995), A comparison of J-values from the composition and photodissociative flux measurement with model calculations, *Geophys. Res. Lett.*, *22*, 1365–1368.

McKenzie, R. L., P. V. Johnston, M. Kotkamp, A. Bittar, and J. D. Hamlin (1992), Solar ultraviolet spectroradiometry in New Zealand: Instrumentation and sample results from 1990, *Appl. Opt.*, *31*, 6501–6509.

McKenzie, R., P. Johnston, A. Hofzumahaus, A. Kraus, S. Madronich, C. A. Cantrell, J. G. Calvert, and R. E. Shetter (2002), Relationship between photolysis frequencies derived from spectroscopic measurements of actinic fluxes and irradiances during the IPMMI campaign, *J. Geophys. Res.*, *107*(D5), 4042, doi:10.1029/2001JD000601.

Michelsen, H. A., R. J. Salawitch, P. O. Wennberg, and J. G. Anderson (1994), Production of $O(^1D)$ from photolysis of O_3, *Geophys. Res. Lett.*, *21*, 2227–2230.

Molina, L. T., and M. J. Molina (1986), Absolute absorption cross sections of ozone in the 185- to 350-nm wavelength range, *J. Geophys. Res.*, *91*, 14,501–14,508.

Monks, P. S., L. J. Carpenter, S. A. Penkett, G. P. Ayers, R. W. Gillet, I. E. Galbally, and C. P. Meyer (1998), Fundamental ozone photochemistry in the remote marine boundary layer: The SOAPEX experiment, measurement and theory, *Atmos. Environ.*, *32*, 3647–3664.

Müller, M. (1994), Messung der aktinischen ultravioletten Strahlung und der Ozon-Photolysefrequenz in der Atmosphäre mittels Filterradiometrie und Spektralradiometrie, Ph.D. thesis, Univ. of Bonn, Bonn, Germany.

Müller, M., A. Kraus, and A. Hofzumahaus (1995), $O_3 \rightarrow O(^1D)$ photolysis frequencies determined from spectroradiometric measurements of solar actinic UV-radiation: Comparison with chemical actinometer measurements, *Geophys. Res. Lett.*, *22*, 679–682.

Olson, J., et al. (1997), Results from the Intergovernmental Panel on Climatic Change Photochemical Model Intercomparison (PhotoComp), *J. Geophys. Res.*, *102*, 5979–5991.

Pfister, G., D. Baumgartner, R. Maderbacher, and E. Putz (2000), Aircraft measurements of photolysis rate coefficients for ozone and nitrogen dioxide under cloudy conditions, *Atmos. Environ.*, *34*, 4019–4029.

Sander, S. P., et al. (2000), Chemical kinetics and photochemical data for use in stratospheric modeling, supplement to evaluation number 12: Update of key reactions, evaluation number 13, *JPL Publ., 00-3*.

Sander, S. P., et al. (2003), Chemical kinetics and photochemical data for use in atmospheric studies: Evaluation number 14, *JPL Publ., 02-25*.

Shetter, R. E., and M. Müller (1999), Photolysis frequency measurements using actinic flux spectroradiometry during the PEM-Tropics mission: Instrumentation description and some results, *J. Geophys. Res.*, *104*, 5647–5661.

Shetter, R. E., et al. (1996), Actinometric and radiometric measurement and modeling of the photolysis rate coefficient of ozone to $O(^1D)$ during the Mauna Loa Observatory Photochemistry Experiment 2, *J. Geophys. Res.*, *101*, 14,631–14,642.

Shetter, R. E., L. Cinquini, B. L. Lefer, S. R. Hall, and S. Madronich (2002), Comparison of airborne measured and calculated spectral actinic flux and derived photolysis frequencies during the PEM Tropics B mission, *J. Geophys. Res.*, *107*, 8234, doi:10.1029/2001JD001320. [printed *108*(D2), 2003]

Shetter, R. E., et al. (2003), Photolysis frequency of NO_2: Measurement and modeling during the International Photolysis Frequency Measurement and Modeling Intercomparison (IPMMI), *J. Geophys. Res.*, *108*(D16), 8544, doi:10.1029/2002JD002932.

Smith, G. D., L. T. Molina, and M. J. Molina (2000), Temperature dependence of $O(^1D)$ quantum yields from the photolysis of ozone between 295 and 338 nm, *J. Phys. Chem.*, *104*, 8916–8921.

Stamnes, K., S.-C. Tsay, W. Wiscombe, and K. Jayaweera (1988), Numerical stable algorithm for discrete-ordinate-method radiative transfer in multiple scattering and emitting layered media, *Appl. Opt.*, *27*, 2502–2509.

Stockwell, W. R., P. Middleton, J. S. Chang, and X. Tang (1990), The second generation regional acid deposition model: Chemical mechanism for regional air quality modelling, *J. Geophys. Res.*, *95*, 16,343–16,367.

Swartz, W. H. (2002), Quantifying photolysis rates in the troposphere and stratosphere, Ph.D. thesis, Univ. of Md., College Park.

Takahashi, K., Y. Matsumi, and M. Kawasaki (1996), Photodissociation processes of ozone in the Huggins band at 308–326 nm: Direct observation of $O(^1D_2)$ and $O(^3P_j)$ products, *J. Phys. Chem.*, *100*, 4084–4089.

Takahashi, K., N. Taniguchi, Y. Matsumi, M. Kawasaki, and M. N. R. Ashfold (1998), Wavelength and temperature dependence of the absolute $O(^1D)$ yield from the 305–329 nm photodissociation of ozone, *J. Chem. Phys.*, *108*, 7161–7172.

Talukdar, R. K., M. K. Gilles, F. Battin-Leclerc, and A. R. Ravishankara (1997), Photolysis of ozone at 308 and 248 nm: Quantum yield of $O(^1D)$ as a function of temperature, *Geophys. Res. Lett.*, *24*, 1091–1094.

Talukdar, R. K., C. A. Longfellow, M. K. Gilles, and A. R. Ravishankara (1998), Quantum yields of $O(^1D)$ in the photolysis of ozone between 289 and 329 nm as a function of temperature, *Geophys. Res. Lett.*, *25*, 143–146.

Trolier, M., and J. R. Wiesenfeld (1988), Relative quantum yield of $O(^1D_2)$ following ozone photolysis between 275 and 325 nm, *J. Geophys. Res.*, *93*, 7119–7124.

WMO Global Ozone Research and Monitoring Project (1985), Atmospheric ozone 1985: Assessment of our understanding of the processes controlling its present distribution and change, vol. 1, *Tech. Rep. 16*, World Meteorol. Organ., Geneva.

Woods, T. N., et al. (1996), Validation of the UARS solar ultraviolet irradiances: Comparison with the Atlas 1 and 2 measurements, *J. Geophys. Res.*, *101*, 9541–9569.

A. Bais, Laboratory of Atmospheric Physics, Aristotle University of Thessaloniki, GR-51124 Thessaloniki, Greece. (abais@auth.gr)

B. Bohn and A. Hofzumahaus, Institut für Chemie und Dynamik der Geosphäre, Institut II: Troposphäre, Forschungszentrum Jülich, D-52425 Jülich, Germany. (b.bohn@fz-juelich.de; a.hofzumahaus@fz-juelich.de)

J. G. Calvert, C. A. Cantrell, G. D. Edwards, S. R. Hall, B. L. Lefer, S. Madronich, G. Pfister, and R. E. Shetter, Atmospheric Chemistry Division, National Center for Atmospheric Research, Boulder, CO 80303, USA. (calvert@acd.ucar.edu; cantrell@acd.ucar.edu; gde@acd.ucar.edu; halls@acd.ucar.edu; lefer@acd.ucar.edu; sasha@acd.ucar.edu; pfister@acd.ucar.edu; shetter@acd.ucar.edu)

G. J. Frost, Cooperative Institute for Research in Environmental Sciences, University of Colorado, Boulder, CO 80303, USA. (gfrost@al.noaa.gov)

E. Griffioen, Meteorological Service of Canada, Toronto, Ontario, Canada M3H 5T4. (erik@nimbus.yorku.ca)

P. Johnston and R. McKenzie, National Institute of Water & Atmospheric Research, NIWA Lauder, PB 50061 Omakau, Central Otago 9182, New Zealand. (p.johnston@niwa.co.nz; r.mckenzie@niwa.co.nz)

W. Junkermann and T. Martin, Institut für Meteorologie und Klimaforschung, Forschungszentrum Karlsruhe, D-82467 Garmisch-Partenkirchen, Germany. (wolfgang.junkermann@imk.fzk.de; timothy.martin@gmx.de)

A. Kraus, Research and Development, Grünenthal GmbH, D-52099 Aachen, Germany. (alexander.kraus@grunenthal.de)

M. Krol, Institute for Marine and Atmospheric Research, NL-3508TA Utrecht, Netherlands. (m.krol@phys.uu.nl)

A. Kylling, Norwegian Institute for Air Research, P. O. Box 100, N-2027 Kjeller, Norway. (arve.kylling@nilu.no)

S. A. Lloyd and W. H. Swartz, Applied Physics Laboratory, Johns Hopkins University, Laurel, MD 20723-6099, USA. (steven.lloyd@jhuapl.edu; bill.swartz@jhuapl.edu)

B. Mayer, Institut für Physik der Atmosphäre, Deutsches Zentrum für Luft- und Raumfahrt, Oberpfaffenhofen, D-82234 Wessling, Germany. (bernhard.mayer@dlr.de)

P. S. Monks, Department of Chemistry, University of Leicester, Leicester, LE1 7RH, UK. (p.s.monks@le.ac.uk)

M. Müller, Dresdner Bank AG, Jürgen-Ponto-Platz 1, D-60301 Frankfurt am Main, Germany. (jo1d@gmx.net)

E. P. Röth, Institut für Chemie und Dynamik der Geosphäre, Institut I: Stratosphäre, Forschungszentrum Jülich, D-52425 Jülich, Germany. (e.p.roeth@fz-juelich.de)

A. Ruggaber, Meteorologisches Institut, Universität München, D-80333 München, Germany. (ruggaber@lrz.uni-muenchen.de)

R. Schmitt, Meteorologie Consult GmbH, D-61479 Glashütten, Germany. (metcon@metcon-us.com)

M. Van Weele, Royal Netherlands Meteorological Institute, NL-3730AE DeBilt, Netherlands. (weelevm@knmi.nl)

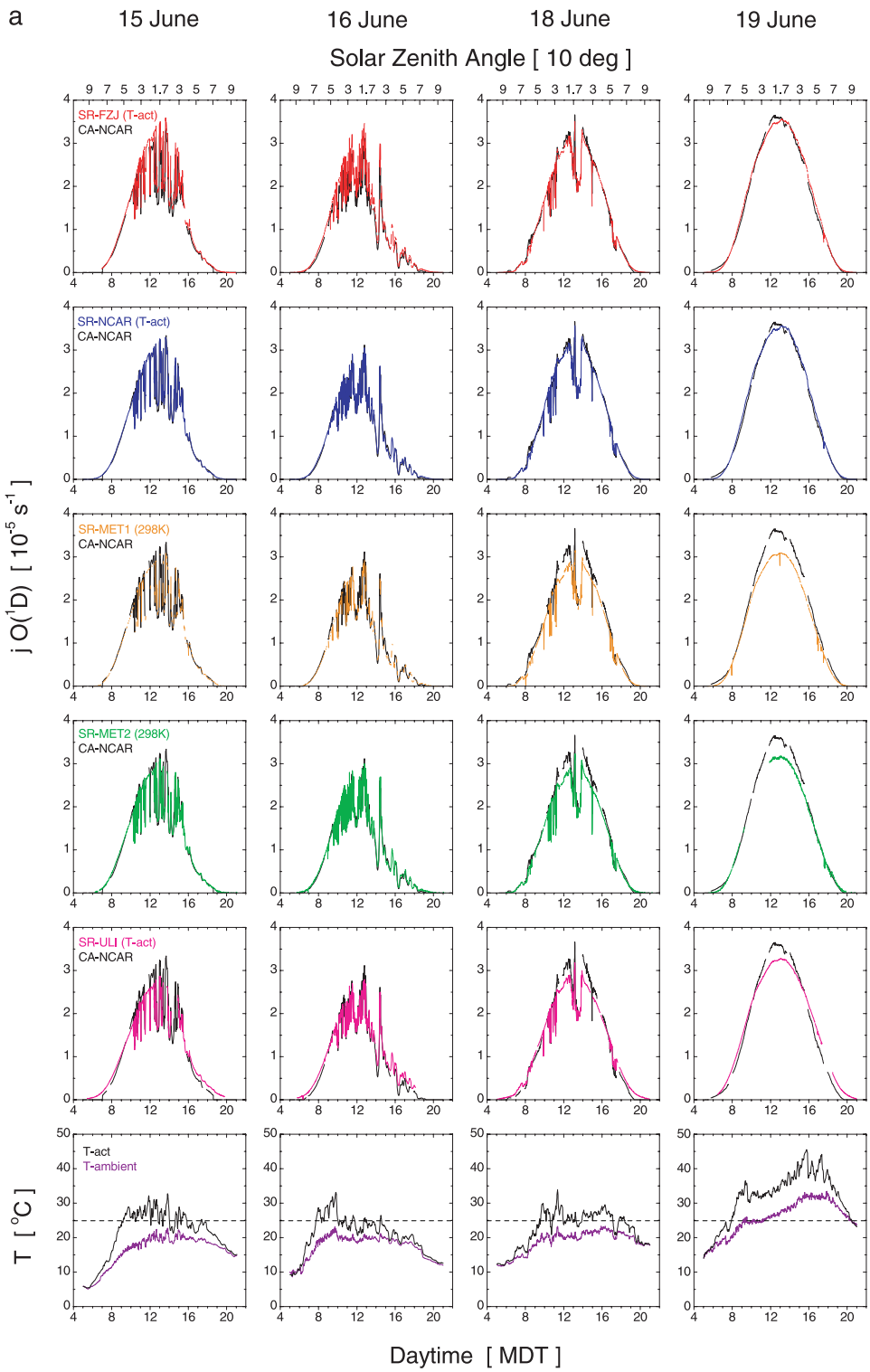

Figure 2. Diurnal profiles of 1-min data of $j(O^1D)$ and temperatures during IPMMI. (a) Comparison of actinic flux spectroradiometers with the chemical actinometer (CA-NCAR). The spectroradiometer data use the ozone absorption cross section $\sigma(\lambda, T)$ from *Molina and Molina* [1986], the quantum yield $\phi(\lambda, T)$ by *Talukdar et al.* [1998], and the temperature of the chemical actinometer. SR-MET1 and SR-MET2 use the quantum yield by *DeMore et al.* [1997] and assume a fixed temperature (298 K) for σ and ϕ. The lowest panel shows measured temperatures of the chemical actinometer and of ambient air. The dashed horizontal line denotes 298 K. (b) Comparison of filter radiometers with the CA-NCAR instrument. All FR data apply to 298 K. Other parameters used for the evaluation of the FR data are given in Table 3.

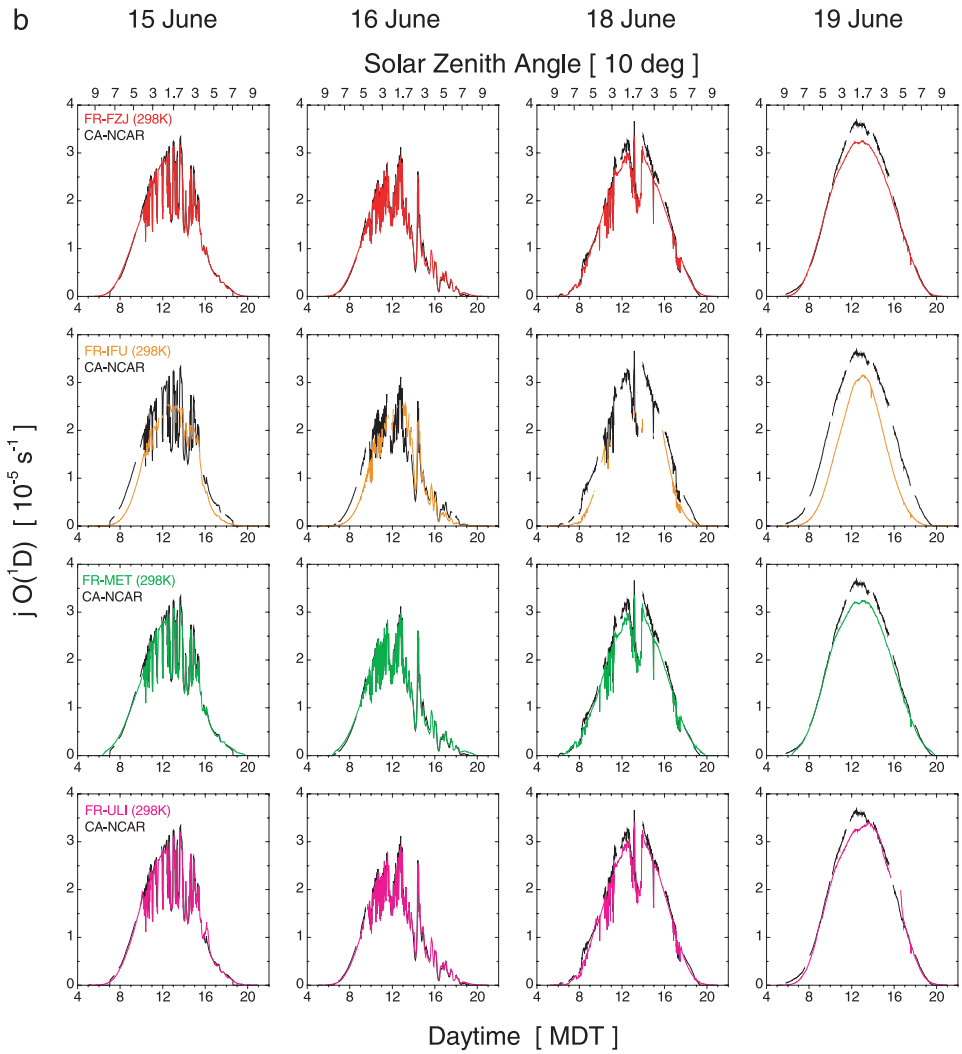

Figure 2. (continued)

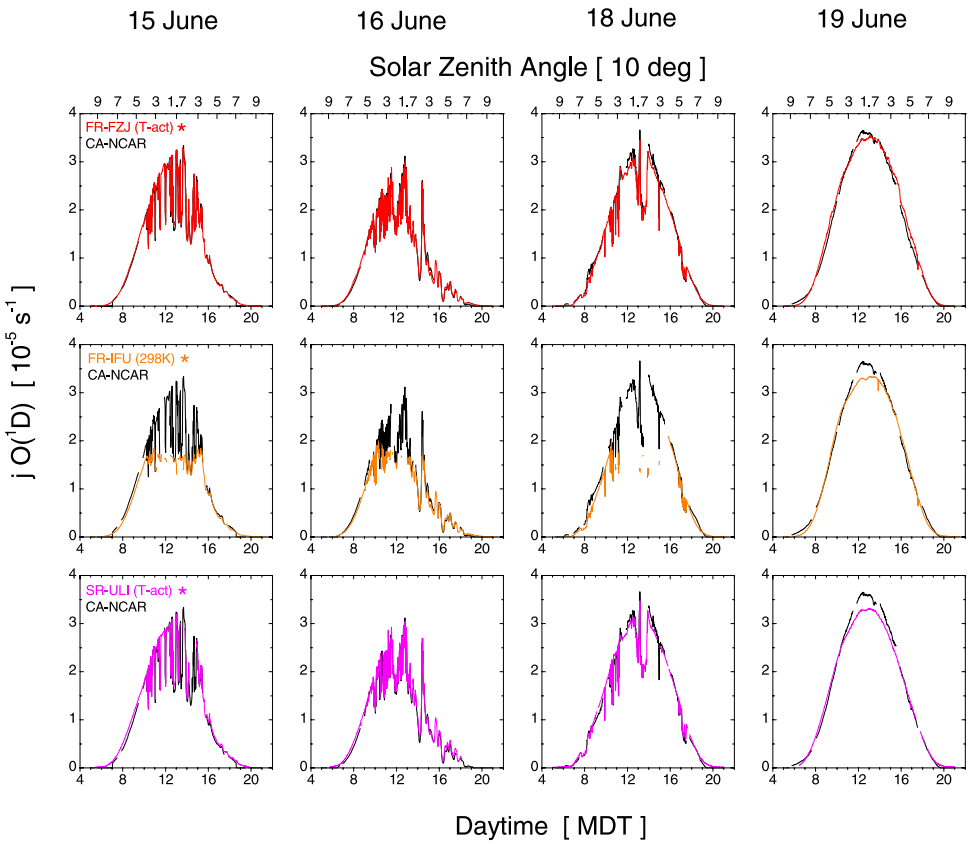

Figure 3. Revised 1-min data of $j(O^1D)$ measured by the instruments FR-FZJ, FR-IFU, and SR-ULI. The revised data, marked with an asterisk, are explained in the text. FR-FZJ* and SR-ULI* use the temperature of the chemical actinometer, whereas FR-IFU* uses 298 K for the evaluation of $j(O^1D)$. The CA-NCAR data are the same as in Figure 2.

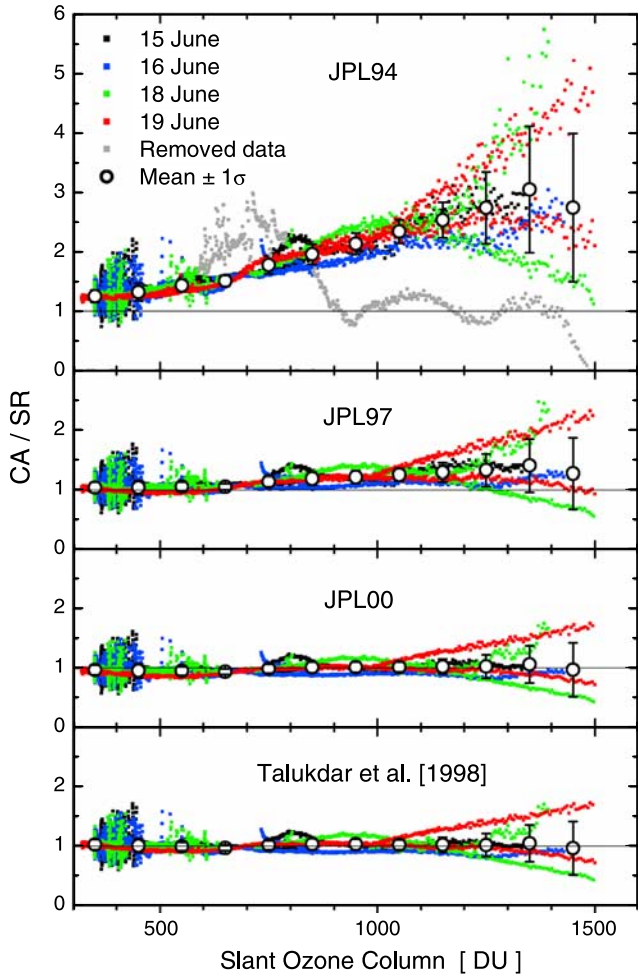

Figure 6. Ratio of $j(O^1D)$ measured by the chemical actinometer and the NCAR spectroradiometer versus the slant ozone column for the days 15–19 June. The spectroradiometer data were evaluated for σ by *Molina and Molina* [1986], different quantum yields (JPL94, JPL97, JPL00, and *Talukdar et al.* [1998]), and the temperature of the actinometer. The open circles represent binned averages over all days for bin widths of 100 DU. The grey symbols in the upper panel have been excluded from the averaging (see text) and are not shown in the other panels.